Finite deformation effects in cellular structures with hyperelastic cell walls

L. Angela Mihai* Alain Goriely†

Abstract

Cellular solids are remarkably strong structures built from seemingly fragile materials. In order to gain new insight into the mechanical behaviour of these omnipresent materials, we analyse the deformation of seamless cellular bodies within the framework of finite strain elasticity and identify behaviours which are not captured under the small strain regime. Assuming that the cell walls are hyperelastic, we devise a mathematical mechanical strategy based on a successive deformation decomposition by which we approximate the large deformation of periodic cellular structures, as follows: (i) firstly, a uniformly deformed state is assumed, as in a compact solid made from the same elastic material; (ii) then the empty spaces of the individual cells are taken into account by setting the cell walls free. For the elastic structures considered here, an isochoric deformation that can be maintained in both compressible and incompressible materials is considered at the first step, then the stresses in this known configuration are used to analyse the free shape problem at the second step where the cell geometry also plays a role. We find that, when these structures are submitted to uniform external conditions such as stretch, shear, or torsion, internal non-uniform local deformations occur on the scale of the cell dimension. For numerical illustration, we simulate computationally the finite elastic deformation of representative model structures with a small number of cells, which convey the complexity of the geometrical and material assumptions required here. Then the theoretical mechanical analysis, which is not restricted by the cell wall material or number of cells, indicates that analogous finite deformation effects are expected also in other physical or computer models.

Key words: cellular structures; elastic material; finite strain deformation; successive deformation decomposition; mathematical mechanical analysis; finite element simulation.

1 Introduction

Cellular solids, by contrast to compact materials, are two or three dimensional bodies divided into cells, the walls of which are made of a solid material capable of undertaking (large) elastic deformations without plastic failure or fracture. Due to their exceptional mechanical efficiency, their realm extends from the primitive natural world to the modern sophisticated engineering, and many familiar materials are cellular, including plant stems, bones, feathers, foams, sponges, and sandwich panels, where strong, light-weight, energy-absorbing structures are desirable [10], [8], [19]. In some 'softer' biogenic or bio-inspired cellular materials, the deformation of the cell walls is entirely elastic (albeit large) and therefore recoverable, but at high strain, opposite cell walls may come into contact with each other and the material collapses by densification (or compaction), while the contacting walls continue to deform elastically as in a compact material [33]. For example, the development of highly flexible stents and scaffolds for soft tissue re-growth in biomedical applications is a rapidly growing multidisciplinary area of biomaterials and tissue engineering, and many foams and sponges designed for cushioning and re-usability can also be found in everyday life as well as in several industrial areas, e.g. microelectronics, aerospace, pharmaceutical and food processes [26].

*School of Mathematics, Cardiff University, Senghennydd Road, Cardiff, CF24 4AG, UK, Email: MihaiLA@cardiff.ac.uk

†Mathematical Institute, University of Oxford, Woodstock Road, Oxford, OX2 6GG, UK, Email: goriely@maths.ox.ac.uk

As for compact materials, it is possible to define an elastic limit for a cellular material: below this limit, the deformation is elastic and can be quite large, while at the elastic limit, the cells collapse by some form of mechanism, such as fracture, plastic deformation, or elastic buckling. Since the rich mechanical behaviour of cellular structures is due to the inextricable relation between the material and the geometry, general results explaining their mechanical behaviour cannot be expected [3]. Nonetheless, important conclusions can be drawn in various special cases by applying suitable strategies.

At low stresses or strains, mathematical models for cellular solids which are based on the physical assumption that the cell walls are linearly elastic with a geometrically nonlinear behaviour are valid. In this context, a comprehensive study of micromechanical models of solid foams is provided by [9].

There is an increasing interest in the nonlinear response of periodic structures capable of large strain deformation, where nonlinear elasticity is expected to play a role. For example, in [20], multiscale stability aspects of the superelastic behavior of hexagonal honeycombs under in-plane compression are analysed, and an in-depth parameter study is performed on the influence of different material laws on the finite strain deformation of honeycombs with perfect and imperfect geometries, while finite element simulations are shown to capture the behavior observed in the experiments; in [29], homogenization estimates for the finite strain effective response of dielectric elastomer composites subject to electromechanical loading conditions are obtained from available estimates for the purely mechanical response combined with a partial decoupling approximation strategy; in [27, 31], a combination of experiments and finite element simulations of elastomeric porous structures show that, by controlling the loading direction, multiple pattern transformations can be induced by buckling, which can then be exploited to design tunable structural materials and devices.

While particular structures seen in experiments can be mimicked computationally by various finite element implementations, there are still many interesting local phenomena that may occur in cellular structures made from nonlinear elastic materials, which are measurable though perhaps not visible, and are yet to be identified and exploited.

Our present goal is to *analyse and compute the deformation of seamless cellular bodies within the framework of finite strain elasticity*, which in principle can provide a complete description of elastic responses of the solid cell walls under loading, and show some interesting behaviours which are not captured in the small strain regime, and thus provide new insight into the rich mechanical response of these structures. In the field of large deformations, finite elasticity covers the simplest case where internal forces (stresses) only depend on the present deformation of the body and not on its history, so it excludes plasticity, viscosity, and damage [1, 12, 24, 30]. Since damage by cell collapse involves additional conditions between the contacting cell walls, we assume that the loading conditions are such that the peak load is below the threshold that will lead to cell closure, and therefore contact between cell walls is not treated here.

Most cellular solids are anisotropic due to the structural distribution of the cells as well as the cell wall material aeolotropic properties. For example, at millimetre scale, plant stems are cellular solids, while at micrometer scale they are fibre reinforced composites. Here, we consider one of the most common features of many cellular solids, namely the orthotropic structural symmetry, whereby the structure has two or three orthogonal axes of symmetry. In our analysis, this is reflected first by the square geometry of the cells while the cell walls are assumed to be isotropic, then also by the orthotropic cell wall material for which the symmetry axes align with those arising from the structural geometry. The assumption of square shaped cells is then sufficient to prove that different local mechanical effects occur when the cell walls are made from a general nonlinear hyperelastic material than when the cell wall material is linearly elastic, which is the main scope of this paper. Interesting finite deformation effects caused by different cell shape geometries are analysed in [23].

For physical plausibility, we require that the cell wall material satisfies the Baker-Ericksen (BE) inequalities stating that *the greater principal stress occurs in the direction of the greater principal stretch* [2], and also the pressure-compression (PC) inequalities stating that *each principal stress is a pressure (compression) or a tension according as the corresponding principal stretch is a contraction or an elongation (extension)* [30, pp. 155-159]. Since these inequalities are satisfied by most elastic materials, as confirmed by experiments and experience, our assumptions are not unduly restrictive.

For linear elastic materials, if μ and κ are the shear and the bulk modulus, respectively, then the PC inequalities take the form $\mu > 0$ and $\kappa > 0$, while BE inequalities are reduced to $\mu > 0$. However, in finite elasticity in general, neither of these two sets of inequalities is implied by the other.

In this context, for thin square and tubular cellular structures made from a nonlinear hyperelastic material, we show that, when these structures are subjected to uniform external conditions, such as stretch, shear, or torsion, internal non-uniform local deformations occur on the scale of the cell dimension. In many cellular structures, *such internal deformations may lead to further changes in the material properties as the deformation progresses*, as seen for example in [23], but their study is non-trivial since the corresponding stresses are non-trivial functions of position and material properties. Nonetheless, the insight gained from the analysis of the deformation for the underlying compact material can provide useful insight into the global behaviour of the structure. Accordingly, we begin our investigation with a uniform deformation, as in a compact material (Section 2), then set the cell walls free by removing the traction constraints at the pre-deformed walls, while the external conditions are maintained (Sections 3, 4, 5, and 6). *This is equivalent to decomposing the large deformation of the cellular structure into two successive deformations: (i) one where a uniform deformation occurs everywhere, as in a compact solid, and (ii) one where the traction constraints at the pre-deformed cell walls are removed, so that the walls deform freely.* By employing this successive decomposition procedure (SDP), we exploit the fact that, under large loading conditions, the deformation of the compact material is potentially closer to that of the cellular structure than the undeformed state, and can be easier to predict, making the final configuration of the structure more tractable. Specifically, for the elastic structures analysed here, an *isochoric deformation* that can be maintained in both compressible and incompressible materials is considered at the first step; then the stresses in this known configuration were used to analyse the *free shape problem* at the second step, where the geometry of the individual cell walls also plays a role.

In this sense, the proposed SDP provides a general mathematical setting applicable to a class of cellular structures made from different hyperelastic materials or containing different numbers of cells, and for which analogous results can be predicted that demonstrate some fundamental differences between the local behaviour of cellular bodies with nonlinear elastic cell walls and those made from linearly elastic materials.

For numerical illustration of the nonlinear mechanical effects under investigation, in Sections 3.1, 4.1, 5.1, and 6.1, finite element simulations of representative model structures with a small number of cells made from a Mooney material are presented, while in Section 7, the effects of increased cell wall thickness in some chosen regions and reinforcing fibres are also considered. For these computer simulations, the size of the cell and the size of the structure are comparable, and therefore the nonlinear mechanical effects at the cell level are visible directly at the structural level. These model simulations were produced using the standard finite element procedure available within then open-source software Finite Elements for Biomechanics (FEBio) environment [17], and are intended as a supplement to show how local nonlinear effects appear in some model structures that convey the complexity of the geometrical and material assumptions required here. Then, in the corresponding sections, it is explained how the (final) non-uniform mechanical deformations predicted by the SDP are captured by the computer models. Undoubtedly, computer implementations based on the proposed SDP are also possible and may yield interesting results, especially in the case of very large deformations, which are often captured less accurately by available methods, as noticed for example by [32]. Although such implementation could make an interesting scientific computing problem in itself, this is beyond the scope of our paper.

While, in addition to the specific geometry, computer simulations require a particular constitutive model for the underlying material to be chosen as well, the proposed successive decomposition procedure indicates that analogous finite deformation effects are to be expected also in similar structural models made from a different elastic material or with a different number of cells.

2 Restrictions on the Material Responses

This Section introduces the key notations and theoretical assumptions and contains sufficient technical material to enable us to carry out the analytical study in the subsequent sections. Before we examine the elastic behaviour of cellular structural materials, we establish some useful results on simple deformations of homogeneous materials which will play an important role in the deformation of cellular structures.

2.1 Extension or Compression of a Hyperelastic Body

For a homogeneous isotropic hyperelastic material subject to the triaxial stretch:

$$x_1 = \lambda_1 X_1, \qquad x_2 = \lambda_2 X_2, \qquad x_3 = \lambda_3 X_3, \tag{2.1}$$

where $\mathbf{X} = [X_1, X_2, X_3]^T$ and $\mathbf{x} = [x_1, x_2, x_3]^T$ denote the reference and current coordinates, respectively, and $\{\lambda_i\}_{i=1,2,3}$ are strictly positive constants, the Cauchy stress tensor $\boldsymbol{\sigma} = (\sigma_{ij})_{i,j=1,2,3}$ has the non-zero components:

$$\sigma_{ii} \;=\; \beta_0 + \beta_1 \lambda_i^2 + \beta_{-1} \lambda_i^{-2}, \qquad i = 1, 2, 3,$$

where the response coefficients $\{\beta_i\}_{i=-1,0,1}$ are scalar functions of the strain invariants:

$$I_1 = \lambda_1^2 + \lambda_2^2 + \lambda_3^2, \quad I_2 = \lambda_1^2\lambda_2^2 + \lambda_2^2\lambda_3^2 + \lambda_3^2\lambda_1^2, \quad I_3 = \lambda_1^2\lambda_2^2\lambda_3^2.$$

In particular, for a hyperelastic body under uniaxial tension acting in the second direction, the Cauchy stress takes the form:

$$\boldsymbol{\sigma} = \begin{bmatrix} 0 & 0 & 0 \\ 0 & T & 0 \\ 0 & 0 & 0 \end{bmatrix}. \tag{2.2}$$

In this case, it is known that the corresponding deformation is a simple extension in the direction of the (positive) tensile force, whereby the ratio between the tensile strain and the strain in the orthogonal direction is greater than one, if and only if the Baker-Ericksen (BE) inequalities stating that *the greater principal stress occurs in the direction of the greater principal stretch* hold [2, 18].

In other words, the deformation corresponding to (2.2), where $T > 0$, has the form (2.1) where $\lambda_2 > \lambda_1 = \lambda_3 > 0$ if and only if the following adsciticious inequalities hold:

$$\text{BE:} \qquad \beta_1 \lambda_i^2 \lambda_j^2 - \beta_{-1} > 0, \quad \text{for} \quad i, j = 1, 2, 3,\ i \neq j. \tag{2.3}$$

In the special case when this deformation is isochoric, *i.e.* $I_3 = 1$, the axial stretches take the form $\lambda_2 = \lambda$ and $\lambda_1 = \lambda_3 = 1/\sqrt{\lambda}$, and the non-zero component of the Cauchy stress is:

$$\sigma_{22} \;=\; (\lambda\beta_1 - \beta_{-1}) \left(\lambda - \frac{1}{\lambda^2}\right).$$

For this deformation, the BE inequalities are equivalent to:

$$\lambda\beta_1 - \beta_{-1} > 0, \tag{2.4}$$

i.e. $\sigma_{22} > 0$ for $\lambda > 1$, and $\sigma_{22} < 0$ for $\lambda < 1$, or in other words, axial tension produces elongation in the same direction, and axial compression produces contraction in the same direction. So the pressure-compression (PC) inequalities [30, p. 155] hold also. We conclude that, for this particular isochoric deformation, BE $\Leftrightarrow$ PC.

In practice, a mean version of the PC conditions is also acceptable, namely [30, pp. 155-156]:

$$\text{PC:} \qquad \sigma_1 \left(1 - \frac{1}{\lambda_1}\right) + \sigma_2 \left(1 - \frac{1}{\lambda_2}\right) + \sigma_3 \left(1 - \frac{1}{\lambda_3}\right) > 0, \tag{2.5}$$

where λ_i and σ_i, $i = 1, 2, 3$, are the principal stretches and the principal stresses, respectively, if not all λ_i are equal to 1.

For the above isochoric deformation, since $\sigma_{11} = \sigma_{33} = 0$, the PC inequality (2.5) becomes:

$$\sigma_{22}\left(1 - \frac{1}{\lambda}\right) = (\lambda\beta_1 - \beta_{-1})\left(\lambda - \frac{1}{\lambda^2}\right)\left(1 - \frac{1}{\lambda}\right) > 0, \tag{2.6}$$

and is clearly equivalent to the BE inequality (2.4). In this case, if $\lambda > 1$, then the deformation is a uniaxial extension in the X_2-direction, and if $\lambda < 1$, then the deformation is a equibiaxial extension in the orthogonal directions.

If an incompressible hyperelastic material is subject to the deformation (2.1), then:

$$\sigma_{ii} \;\; = \;\; -p + \beta_1\lambda_i^2 + \beta_{-1}\lambda_i^{-2}, \qquad i = 1, 2, 3,$$

where p is an arbitrary hydrostatic pressure. In this case, if $\lambda_2 = \lambda$ and $\lambda_1 = \lambda_3 = 1/\sqrt{\lambda}$, then by setting $\sigma_{11} = \sigma_{33} = 0$, we also find that BE $\Leftrightarrow$ PC [30, p. 180].

2.2 Inflation and Compression of a Circular Tube

For an incompressible elastic circular tube with inner radius A, outer radius B, and length L subject to longitudinal extension or compression, the deformation can be written as follows:

$$r = \frac{1}{\sqrt{\lambda}}R, \qquad \theta = \Theta, \qquad z = \lambda Z, \tag{2.7}$$

where (r, θ, z) and (R, Θ, Z) are the cylindrical coordinates for the current and undeformed configuration, respectively, and $l = \lambda L$ is the length of the tube after deformation.

As there is no rotation involved in (2.7), in cylindrical coordinates (r, θ, z) and (R, Θ, Z), the deformation gradient takes the form:

$$\mathbf{F} = \begin{bmatrix} 1/\sqrt{\lambda} & 0 & 0 \\ 0 & 1/\sqrt{\lambda} & 0 \\ 0 & 0 & \lambda \end{bmatrix},$$

i.e. if $\lambda > 1$, then the deformation is a simple extension in the longitudinal direction (elongation), and if $1/\lambda > 1$, then the deformation is an equibiaxial extension in the radial and transverse (tangential) directions (inflation).

In this case, by setting $\sigma_{rr} = \sigma_{\theta\theta} = 0$ in the radial and transverse directions, respectively, the Cauchy stress tensor is equal to:

$$\boldsymbol{\sigma} = \begin{bmatrix} 0 & 0 & 0 \\ 0 & 0 & 0 \\ 0 & 0 & \sigma_{zz} \end{bmatrix},$$

where the non-zero component takes the form:

$$\sigma_{zz} = (\lambda\beta_1 - \beta_{-1})\left(\lambda - \frac{1}{\lambda^2}\right). \tag{2.8}$$

2.3 Simple Shear and the Poynting Effect

When a hyperelastic material is subject to the simple shear deformation:

$$x_1 = X_1 + KX_2, \qquad x_2 = X_2, \qquad x_3 = X_3, \tag{2.9}$$

where $K > 0$ is a constant, the strain invariants are:

$$I_1 = K^2 + 3 = I_2 \qquad \text{and} \qquad I_3 = 1,$$

and, assuming that the planes of shear are free, *i.e.* $\sigma_{33} = 0$, the non-zero stress components are:

$$\sigma_{11} = K^2\beta_1, \qquad \sigma_{22} = K^2\beta_{-1}, \qquad \sigma_{12} = K(\beta_1 - \beta_{-1}).$$

For a unit cube occupying the domain $[0,1]\times[0,1]\times[0,1]$ and deformed by the simple shear (2.9), the normal and tangential tractions on the sheared faces are, respectively:

$$\sigma_n = \sigma_{22}, \qquad \sigma_t = -\sigma_{12}. \tag{2.10}$$

Then, for the deformed cube, the unit normal and tangent vectors on the inclined faces are, respectively:

$$\mathbf{n} = \pm\frac{1}{\sqrt{1+K^2}}\begin{bmatrix} 1 \\ -K \\ 0 \end{bmatrix}, \qquad \mathbf{t} = \pm\frac{1}{\sqrt{1+K^2}}\begin{bmatrix} K \\ 1 \\ 0 \end{bmatrix}.$$

On these faces, the corresponding normal and shear tractions are, respectively:

$$\sigma_n = \sigma_{22} - \frac{K\sigma_{12}}{1+K^2}, \qquad \sigma_t = \frac{\sigma_{12}}{1+K^2}. \tag{2.11}$$

For a square section of a material deformed by simple shear, the normal and tangential directions on the external faces are indicated in Figure 1.

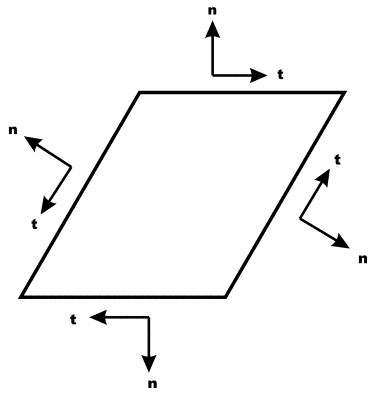

Figure 1: Simple shear of a square section of a material, showing the normal and tangent unit vectors on the external faces.

For the shear deformation (2.9) also, the principal stresses take the form:

$$\sigma_i = \beta_0 + \beta_1\lambda_i^2 + \beta_{-1}\lambda_i^{-2}, \qquad i = 1,2,3,$$

where $\{\lambda_i\}_{i=1,2,3}$ are the principal stretches, given by:

$$\lambda_1^2 = 1 + \frac{K^2 + K\sqrt{K^2+4}}{2} = \lambda^2, \quad \lambda_2^2 = 1 + \frac{K^2 - K\sqrt{K^2+4}}{2} = \lambda^{-2}, \quad \lambda_3^2 = 1. \tag{2.12}$$

Then, assuming that $\sigma_3 = 0$, the remaining principal stresses are:

$$\begin{aligned} \sigma_1 &= \beta_1\frac{K^2 + K\sqrt{K^2+4}}{2} + \beta_{-1}\frac{K^2 - K\sqrt{K^2+4}}{2}, \\ \sigma_2 &= \beta_1\frac{K^2 - K\sqrt{K^2+4}}{2} + \beta_{-1}\frac{K^2 + K\sqrt{K^2+4}}{2}. \end{aligned}$$

Let $\{\mathbf{e}_i\}_{i=1,2,3}$ denote the unit vectors in the Lagrangean directions $\{X_i\}_{i=1,2,3}$, respectively, and $\{\mathbf{v}_i\}_{i=1,2,3}$ be the unit vectors in the principal (Eulerian) directions of the deformation (2.9) satisfying $\mathbf{B}\mathbf{v}_i = \lambda_i\mathbf{v}_i$, $i = 1,2,3$, where $\mathbf{B} = \mathbf{F}\mathbf{F}^T$ is the left Cauchy-Green strain tensor. Explicitly:

$$\mathbf{v}_1 = \mathbf{e}_1\cos\alpha + \mathbf{e}_2\sin\alpha, \qquad \mathbf{v}_2 = -\mathbf{e}_1\sin\alpha + \mathbf{e}_2\cos\alpha, \qquad \mathbf{v}_3 = \mathbf{e}_3, \tag{2.13}$$

where the angle α satisfies:

$$\tan\alpha = \frac{2}{K+\sqrt{K^2+4}}, \qquad 0 \le \alpha \le \frac{\pi}{4}. \tag{2.14}$$

Then the following decomposition holds:

$$\mathbf{B} = \mathbf{R}\mathbf{U}^2\mathbf{R}^T, \tag{2.15}$$

where

$$\mathbf{R} = \begin{bmatrix} \cos\alpha & -\sin\alpha & 0 \\ \sin\alpha & \cos\alpha & 0 \\ 0 & 0 & 1 \end{bmatrix} \qquad \text{and} \qquad \mathbf{U} = \begin{bmatrix} \lambda & 0 & 0 \\ 0 & \lambda^{-1} & 0 \\ 0 & 0 & 1 \end{bmatrix},$$

and by the Polar Decomposition Theorem, $\mathbf{F} = \mathbf{R}\mathbf{U}$.

This decomposition is important for the geometrical interpretation of the shear deformation [24, pp. 101-104]. In particular, the circle inscribed in the unit square $[0,1]\times[0,1]$ deforms into an ellipse with the major axis along the principal direction $\mathbf{v}_1$ and eccentricity λ^2. Moreover, since:

$$\frac{1}{K+1} < \tan\alpha < 1 \qquad \text{for} \quad 0 < K < \infty,$$

the principal axes are situated between the diagonals of the undeformed and sheared square, respectively.

For a square section of a material deformed by simple shear, the principal directions before and after the deformation are represented in Figure 2.

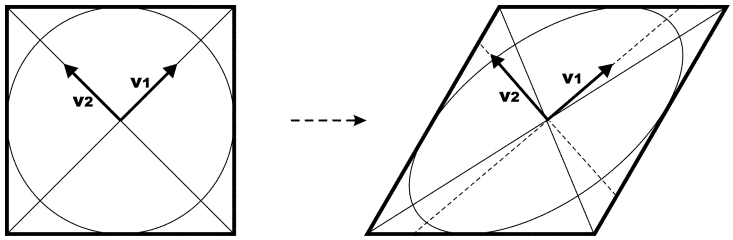

Figure 2: Simple shear of a square section of a material, showing the principal directions before (left) and after (right) deformation.

In the limiting case when $K \to 0$, since $\tan\alpha \to 1$, the Eulerian directions are along the diagonals of the unit square in the undeformed state, while if $K \to \infty$, then $\tan\alpha \to 1/(K+1)$, *i.e.* the first principal direction is effectively on the longer diagonal of the deformed square.

Conversely, by the decomposition (2.15), any biaxial stretch of the form:

$$x_1 = \lambda X_1, \qquad x_2 = \frac{1}{\lambda}X_2, \qquad x_3 = X_3, \tag{2.16}$$

where $\lambda > 1$, is equivalent to a simple shear with amount of shear $K = (\lambda^2-1)/\lambda$ at a relative angle α, such that $\tan\alpha = 1/\lambda$ (see Figure 3).

Note that, for the simple shear (2.9) and the biaxial stretch (2.16), straight parallel lines remain straight and parallel, while in simple shear, the length in the $\mathbf{e}_1$ direction is also preserved. In the linear elastic limit, $\lambda = 1+\epsilon$, where $0 < \epsilon \ll 1$, and the biaxial stretch (2.16) is equivalent to a simple shear at a relative angle $\alpha = \pi/4$.

In the general case, it can be verified that:

$$\sigma_1 - \sigma_3\lambda_1^{-2} = \beta_0\left(1-\lambda_1^{-2}\right) + \beta_1\left(\lambda_1^2 - \lambda_1^{-2}\right),$$

where, assuming that the BE inequalities are valid, the left hand-side is positive, and since the brackets on the right hand-side are also positive, the following generalised empirical inequalities may hold [21, 22]:

$$\text{GEI:} \qquad \beta_0 \le 0 \qquad \text{and} \qquad \beta_1 > 0. \tag{2.17}$$

Then the following situations are possible:

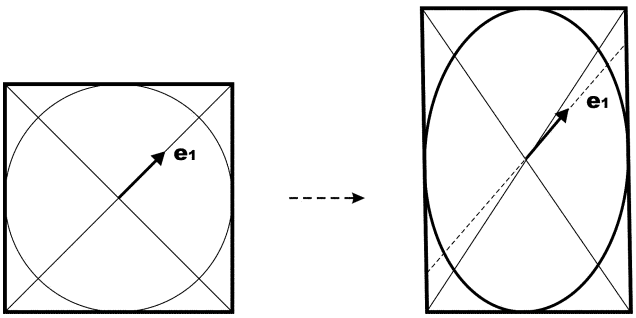

Figure 3: Biaxial stretch of a square section of a material, showing the simple shear direction before (left) and after (right) deformation.

(i) If $\beta_{-1} < 0$, then $\sigma_{22} < 0$, *i.e.* a compressive stress is necessary to prevent the plane sections perpendicular to the X_2-direction from moving in the positive direction of X_2 (the positive Poynting effect).

On the sheared faces, $\sigma_t < 0$, *i.e.* the tangential traction is compressive, and $\sigma_n < 0$, *i.e.* the normal traction is also compressive.

On the inclined faces, $\sigma_t > 0$, *i.e.* the tangential traction is tensile, and $\sigma_n < 0$, *i.e.* the normal traction is compressive.

In the principal directions $\mathbf{v}_1$ and $\mathbf{v}_2$, $\sigma_1 > 0$ and $\sigma_2 < 0$, *i.e.* the deformation is an extension in the first direction and a compression in the second direction, which by the PC inequalities is consistent with the fact that $\lambda_1 = \lambda > 1$ and $\lambda_2 = 1/\lambda < 1$.

(ii) If $\beta_1 > \beta_{-1} > 0$, so that $\sigma_{12} > 0$, then $\sigma_{22} > 0$, *i.e.* a tensile stress is required to prevent the plane sections perpendicular to the X_2-direction from moving in the negative direction of X_2 (the negative Poynting effect).

In this case, on the sheared faces, $\sigma_t < 0$ and $\sigma_n > 0$, while on the inclined faces, $\sigma_t > 0$ and:

$$\sigma_n \leq 0 \quad \text{for} \quad K^2 \leq \frac{\beta_1 - 2\beta_{-1}}{\beta_{-1}},$$
$$\sigma_n > 0 \quad \text{for} \quad K^2 > \frac{\beta_1 - 2\beta_{-1}}{\beta_{-1}}.$$

In the principal directions, $\sigma_1 > 0$, *i.e.* the deformation is an extension in the first direction, which agrees with the fact that $\lambda_1 = \lambda > 1$, while in the second direction:

$$\sigma_2 \leq 0 \quad \text{for} \quad K \leq \frac{\beta_1 - \beta_{-1}}{\sqrt{\beta_1 \beta_{-1}}},$$
$$\sigma_2 > 0 \quad \text{for} \quad K > \frac{\beta_1 - \beta_{-1}}{\sqrt{\beta_1 \beta_{-1}}}.$$

Since $\lambda_2 = 1/\lambda < 1$, *i.e.* the second principal stretch is a contraction, if the PC inequalities hold, then by the above inequalities, the shear parameter K may only take values such that the second principal stress is compressive, *i.e.* $\sigma_2 \leq 0$. We denote the corresponding maximum value for K by:

$$K_c = \frac{\beta_1 - \beta_{-1}}{\sqrt{\beta_1 \beta_{-1}}}. \tag{2.18}$$

However, by the mean version of the PC conditions (2.5), the second principal stress may satisfy the following weaker inequality $\sigma_2 \leq \sigma_1/\lambda$.

(iii) If $\beta_{-1} = 0$, then $\sigma_{22} = 0$, *i.e.* the plane sections perpendicular to the X_2-direction maintain their original position, and the analysis is similar to that of case (i).

2.4 Simple Torsion of a Cylinder as Simple Shear

For an incompressible elastic cylinder subject to simple torsion, the deformation in cylindrical coordinates takes the form [13], [24, p. 114]:

$$r = R, \qquad \theta = \Theta + \tau Z, \qquad z = Z, \tag{2.19}$$

where τ is the twist per unit length of the deformed cylinder, and (r, θ, z) and (R, Θ, Z) are the cylindrical coordinates for the current and undeformed configuration, respectively. During this deformation, the plane section at $Z = 0$ remains fixed, while each plane section normal to the central axis remains plane and the radius R rotates by an angle τZ.

In cylindrical coordinates, the deformation gradient is:

$$\mathbf{F} = \begin{bmatrix} 1 & 0 & 0 \\ 0 & 1 & \tau R \\ 0 & 0 & 1 \end{bmatrix},$$

hence the simple torsion (2.19) can be regarded as a simple shear in the transverse direction Θ (with shear parameter $\tau R > 0$). Under this deformation, the positive Poynting effect occurs if $\sigma_{zz} < 0$, *i.e.* the cylinder tends to elongate and a compressive stress in the axial direction is necessary to keep its length fixed, while the negative Poynting effect is obtained if $\sigma_{zz} > 0$, i.e. the cylinder tends to shorten and a tensile stress in the axial direction is required to maintain the same length.

3 Extension Compression of a Cellular Structure (or How to be Flexible)

We consider a thin square section of an elastic material where parts of the material have been removed to create a uniform network of disconnected square cells, as depicted for example in Figure 4. Assuming that the edges of the squares are parallel to the directions X_1 and X_2, respectively, we first study the deformation of this cellular structure when two opposite external surfaces are subject to the uniform stretch:

$$x_1 = X_1, \qquad x_2 = \lambda X_2, \qquad x_3 = \frac{1}{\lambda} X_3, \tag{3.1}$$

where $\lambda > 0$ is constant, while all the other surfaces deform freely.

(a) 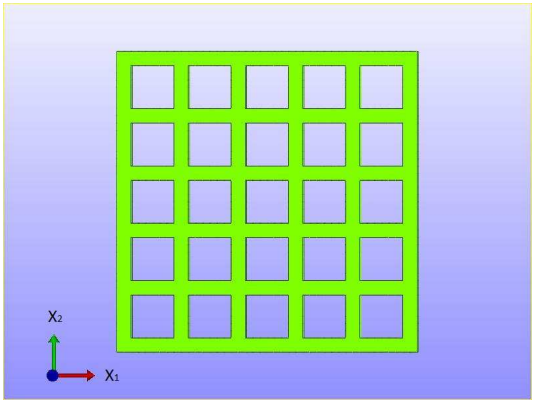

(b) 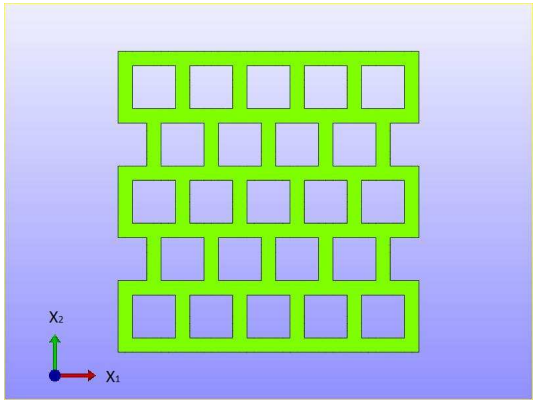

Figure 4: Undeformed square section of cellular material with (a) stacked and (b) staggered cell distribution.

We identify the direction X_1 with the horizontal direction, and the orthogonal direction X_2 with the vertical direction, and assume that the opposite external faces where the uniform stretch (3.1) is prescribed lie horizontally. Then $\lambda > 1$ corresponds to a vertical elongation and $\lambda < 1$ corresponds to a vertical contraction.

We further assume that, when the cell wall material is subject to uniaxial tension, elongation in one direction is accompanied by biaxial contraction in the orthogonal directions, and similarly, when the cell wall is under uniaxial compression, contraction in one direction is accompanied by biaxial extension in the orthogonal directions. This assumption is consistent with the analysis in Section 2.1.

Under these external conditions, the deformation inside the cellular structure is non-trivial as the corresponding stresses depend on both the position and the underlying material properties. Remarkably, the insight gained from the analysis of the uniform deformation of the elastic material contains useful information on the global behaviour of these structures. To see this:

(i) We assume first that the homogeneous deformation (3.1) occurs throughout the cellular structure, as in a compact material.

(ii) Then we set the cell walls free, and thus take into account the empty spaces inside the cells, while the external conditions (3.1) on the specified boundaries are maintained.

This is equivalent to decomposing the deformation of the cellular material into two successive deformations: (i) one where the homogeneous (affine) deformation occurs everywhere, as in a compact solid, and (ii) one which uses the homogeneous configuration as the reference state and where the surface constraints at the cell walls are removed, so that these walls may deform freely (see Figure 5).

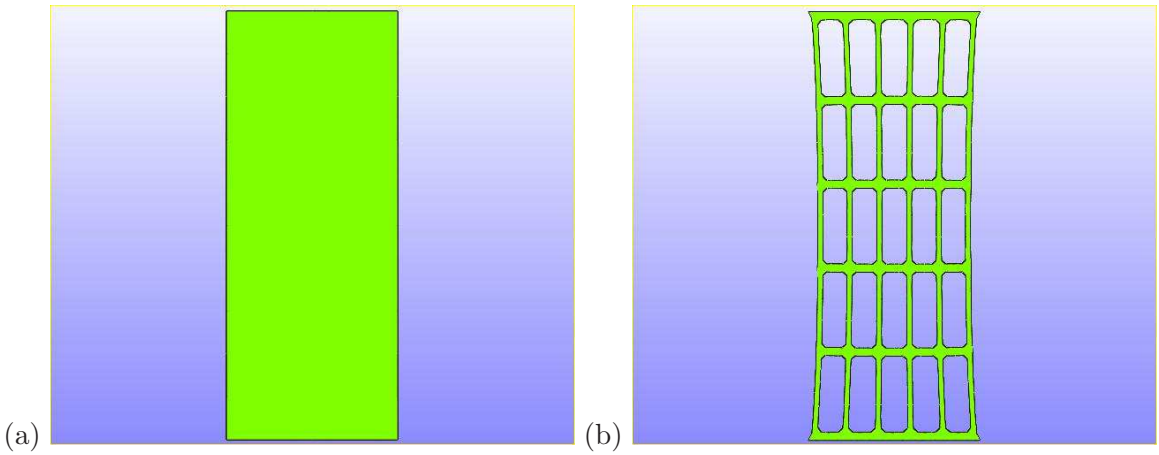

Figure 5: Square section of cellular material after (a) the first and (b) the second step of the successive decomposition procedure when $\lambda > 1$.

Successive Decomposition Procedure (SDP) of Large Deformations in Cellular Structures. The successive deformation decomposition that we propose for large deformations in cellular structures can be formally written as follows: if $\mathbf{x}' = \boldsymbol{\chi}'(\mathbf{X}) \in \mathbb{R}^3$ describes the first deformation at step (i), and $\mathbf{x} = \boldsymbol{\chi}(\mathbf{X}) \in \mathbb{R}^3$ is the final deformation of step (ii), written with respect to the material configuration $\mathcal{B}_0$, then the deformation:

$$\mathbf{x}'' = \boldsymbol{\chi}''(\mathbf{x}') = \boldsymbol{\chi}\left(\boldsymbol{\chi}'^{-1}(\mathbf{x}')\right)$$

maps the deformed state $\mathcal{B}'$ to the final configuration $\mathcal{B}$ (see Figure 6).

Let $\mathbf{F} = d\boldsymbol{\chi}(\mathbf{X})/d\mathbf{X}$, $\mathbf{F}' = d\boldsymbol{\chi}'(\mathbf{X})/d\mathbf{X}$, and $\mathbf{F}'' = d\boldsymbol{\chi}''(\mathbf{x})/d\mathbf{x}$ be the corresponding deformation gradients, such that $\det \mathbf{F}' > 0$ and $\det \mathbf{F}'' > 0$, *i.e.* the mappings $\boldsymbol{\chi}'$ and $\boldsymbol{\chi}''$ are invertible and orientation preserving. Then, by the chain rule, the following compatible multiplicative decomposition holds:

$$\mathbf{F} = \mathbf{F}''\mathbf{F}'. \tag{3.2}$$

Remark 3.1 *The multiplicative decomposition (3.2) is formally the same as those found in constitutive theories of thermoelasticity, elastoplasticity, and growth kinematics [16], but it is fundamentally*

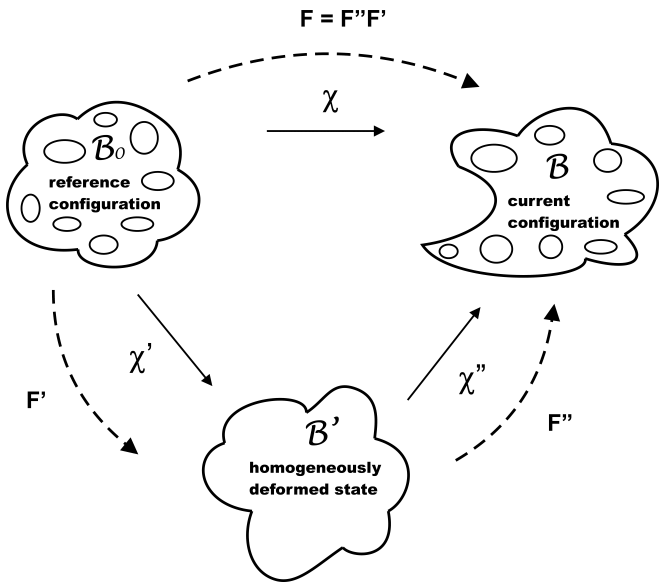

Figure 6: Schematic representation of the successive decomposition procedure.

different as here all configurations are compatible in the sense that they are obtained by finite deformations of the same elastic material. True, although the homogeneous configuration at the end of step (i) may not physically occur in practice, it is nevertheless possible for the cell walls to assume such a state under suitable loading conditions. In fact, homogeneous (affine) deformations are the only universal deformations, i.e. *they can be maintained in every homogeneous isotropic hyperelastic material [6,28], [24, pp 244-246], [30, p 336-337], and are especially useful, since for a homogeneous elastic body subject to a given affine deformation, the traction induced on the boundary can be determined (inverse problem). Then the (constant) stresses for this known configuration can be used to analyse the 'free shape' (inverse) problem at step (ii) [30, p. 130], where the particular geometry of the cell walls also plays a role.*

Note that, at the second step, where the prescribed external conditions are maintained and the internal surfaces are set free, the problem is fully determined due to the fact that the cellular structure is made from a single piece of material.

Furthermore, if a cellular structure is made from a linearly elastic material under the external conditions, then the homogeneous deformation at step (i) can be maintained by forces acting at the ends of the cell walls only, while the tractions at the cell wall faces are zero, hence the second step (ii) is not required.

In this context, the proposed SDP provides a general mathematical framework demonstrating some fundamental differences between the local behaviour of cellular structures with nonlinear elastic cell walls and those made of linearly elastic materials when subjected to some of the most common loading conditions.

For a vertical elongation ($\lambda > 1$):

(i) At the first step of the SDP, the material deforms by the uniform elongation (3.1) with the (constant) deformation gradient:

$$\mathbf{F}' = \begin{bmatrix} 1 & 0 & 0 \\ 0 & \lambda & 0 \\ 0 & 0 & 1/\lambda \end{bmatrix}.$$

(ii) At the second step, for a pre-deformed vertical wall, the boundary conditions (3.1) are maintained at the horizontal ends and the vertical sides are set free. Assuming that the cell walls are sufficiently long and thin, the Cauchy stress for the vertical wall in the final configuration may

be approximated by a uniaxial tension (2.2), with the corresponding deformation gradient of the form:

$$\mathbf{F} = \begin{bmatrix} \lambda_1 & 0 & 0 \\ 0 & \lambda & 0 \\ 0 & 0 & \lambda_1 \end{bmatrix}.$$

Taking into account the above assumption that, if a cell wall is subject to a uniaxial tension (2.2), then elongation in one direction is accompanied by biaxial contraction in the orthogonal directions, we deduce that $0 < \lambda_1 < 1 < \lambda$.

Then, by the multiplicative decomposition (3.2), the deformation gradient for the vertical wall at the second step is:

$$\mathbf{F}'' = \begin{bmatrix} \lambda_1 & 0 & 0 \\ 0 & 1 & 0 \\ 0 & 0 & \lambda\lambda_1 \end{bmatrix},$$

i.e. the pre-deformed vertical wall remains stretched in the vertical direction and contracts in the horizontal direction. However, due to the geometry of the cell wall, the horizontal contraction may be small.

For a pre-stretched horizontal wall, when all the normal tensile constraints at its surfaces are removed, if the deformation gradient in the horizontal direction is approximated by that for the vertical wall which it intersects, while in the other directions the wall is free, then the pre-deformed horizontal wall contracts in both the horizontal (longitudinal) and the vertical (transverse) directions.

The longitudinal contraction in the horizontal wall acts also as a transverse force for the vertical walls which it intersects. It is shown in [7] that, when a circular bar of an incompressible material is finitely extended or compressed in the axial direction, and subject to a small transverse load at one end while the other end is held fixed, the bar will first bend until the compressive load reaches a critical value at which the bar becomes unstable. By analogy, we expect that a pre-stretched vertical wall intersecting a horizontal wall will bend.

At the structural level, assuming symmetry of the structure around the vertical and horizontal axes, the vertical walls which are held fixed at their horizontal ends will bend towards the vertical axis. Thus the pre-deformed structure will contract non-uniformly in the horizontal direction, with the maximum contraction along the horizontal axis.

For a vertical contraction ($0 < \lambda < 1$):

(i) In the first step of the SDP, the material deforms by the uniform contraction (3.1).

(ii) In the second step, for every pre-deformed vertical wall, the boundary conditions (3.1) are maintained at the horizontal ends, and when the vertical faces are set free and thus the compressive normal traction constraints are removed, the wall either expands horizontally, buckles, or bends.

For a pre-compressed horizontal wall, when the normal traction constraints are removed, the wall extends both horizontally and vertically.

At the structural level, as every horizontal wall extends horizontally, while the vertical walls buckle or bend, the pre-deformed cellular material will first expand horizontally. However, since a symmetric solution around the vertical axis can lead to instability of the central vertical walls, this may eventually produce a non-symmetric deformation in the structure, causing the horizontal walls to come into contact during the shear type deformation of the cells.

In the linear elastic limit $\lambda \to 1$, the axial load approaches zero, and an almost uniform deformation is obtained.

3.1 Elongation or Contraction of a Cellular Structure of Mooney Material

To illustrate the above argument, we present a set of numerical examples for cellular structures made of a Mooney hyperelastic material described by the stored energy density:

$$\mathcal{W} = \frac{\mu_1}{2}\left(I_3^{-1/3}I_1 - 3\right) + \frac{\mu_2}{2}\left(I_3^{-2/3}I_2 - 3\right) + \frac{\kappa}{2}\left(I_3^{1/2} - 1\right)^2, \tag{3.3}$$

where $\mu = \mu_1 + \mu_2 > 0$ is the shear modulus and $\kappa > 0$ is the bulk modulus. In the incompressible case, the material corresponds to the classical Mooney-Rivlin model.

When an elastic body of material (3.3) is subject to the simple extension (2.1) with $\lambda_1 = \lambda > 1$ and $\lambda_2 = \lambda_3 = 1/\sqrt{\lambda}$, the non-zero components of the Cauchy stress are:

$$\begin{aligned}
\sigma_{11} &= \frac{2\mu_1}{3}\left(\lambda^2 - \frac{1}{\lambda}\right) + \frac{2\mu_2}{3}\left(3\lambda - \lambda^2 - \frac{2}{\lambda}\right),\\
\sigma_{22} &= \frac{\mu_1}{3}\left(\frac{1}{\lambda} - \lambda^2\right) + \frac{\mu_2}{3}\left(3\lambda + \frac{3}{\lambda^2} - 2\lambda^2 - \frac{4}{\lambda}\right),\\
\sigma_{33} &= \sigma_{22}.
\end{aligned}$$

In this case, the BE inequalities are equivalent to (2.4), with $\beta_1 = \mu_1$ and $\beta_{-1} = -\mu_2$. As $\mu_1 + \mu_2 > 0$, assuming that $\mu_1 > 0$, if $\mu_2 > 0$, then (2.4) holds for all $\lambda > 1$, and if $\mu_2 < 0$, then (2.4) is valid for all $\lambda > 1 > -\mu_2/\mu_1$. Therefore BE are satisfied for all $\lambda > 1$.

One can verify that $\mu_1 + \mu_2 > 0$, together with $\mu_1 > 0$, implies also:

$$\sigma_{11}\left(1 - \frac{1}{\lambda}\right) + 2\sigma_{22}\left(1 - \sqrt{\lambda}\right) > 0,$$

i.e. the PC inequality (2.5) is satisfied for all $\lambda > 1$. This is to be expected following the analysis given in Section 2.1.

For the numerical simulations, we first consider a single cell wall of size $1 \times 3 \times 1$, subject to longitudinal extension or compression while the side walls are free. The constitutive parameters for the Mooney material are chosen $\mu_1 = 1.2$ MPa, $\mu_2 = 0.2$ MPa and $\kappa = 100$ MPa (model 1). In the graphical representations, the finite element mesh for the deformed elastic wall is also shown.

For a cell wall under large longitudinal extension, or compression, the deformation and stresses are illustrated in Figure 7. Note that, in extension, the cell wall contracts horizontally far away from the fixed boundaries, while in compression, the wall expands horizontally, as suggested also by the stresses in Figure 7 (a) and (b), respectively. In these numerical examples, when the cell wall was compressed vertically, a small horizontal displacement was also prescribed at the top horizontal face to obtain the post-buckled solution (see also [15], pp. 562-3).

Next, we take a thin square section of a cellular structure where the horizontal external faces are subject to uniaxial extension (or compression), while the other faces deform freely. For visual clarity, in the graphical representations, the contour of the cell walls is included while the finite element mesh for the individual cell walls is omitted.

For a cellular section of side one, with stacked or staggered cells and subject to large vertical extension ($\lambda > 1$) or compression ($\lambda < 1$), the non-uniform deformation and stresses in the horizontal and vertical directions are illustrated in Figure 8 and 10, respectively. As predicted by the SDP, when $\lambda > 1$, the vertical walls bend and the horizontal walls contract horizontally, and when $\lambda < 1$, the vertical walls buckle.

Locally, under vertical extension, the cell walls tend to elongate in the vertical direction and contract in the horizontal direction. This behaviour is similar to that of the compact cell wall under analogous external conditions in Figure 7.

For the cellular material under vertical compression, the vertical walls buckle and the cells suffer a shear type deformation. In Figure 9, the unstable symmetric deformation, whereby the horizontal walls extends horizontally, is also shown as an intermediate state obtained during the numerical procedure, before the buckled solution is found. As in the case of single cell wall, a small horizontal displacement was also prescribed at the top horizontal face to obtain the numerical solution.

In Figure 10, the horizontal walls bend at the intersection with the vertical walls, and the initially quadrilateral cells eventually become hexagonal.

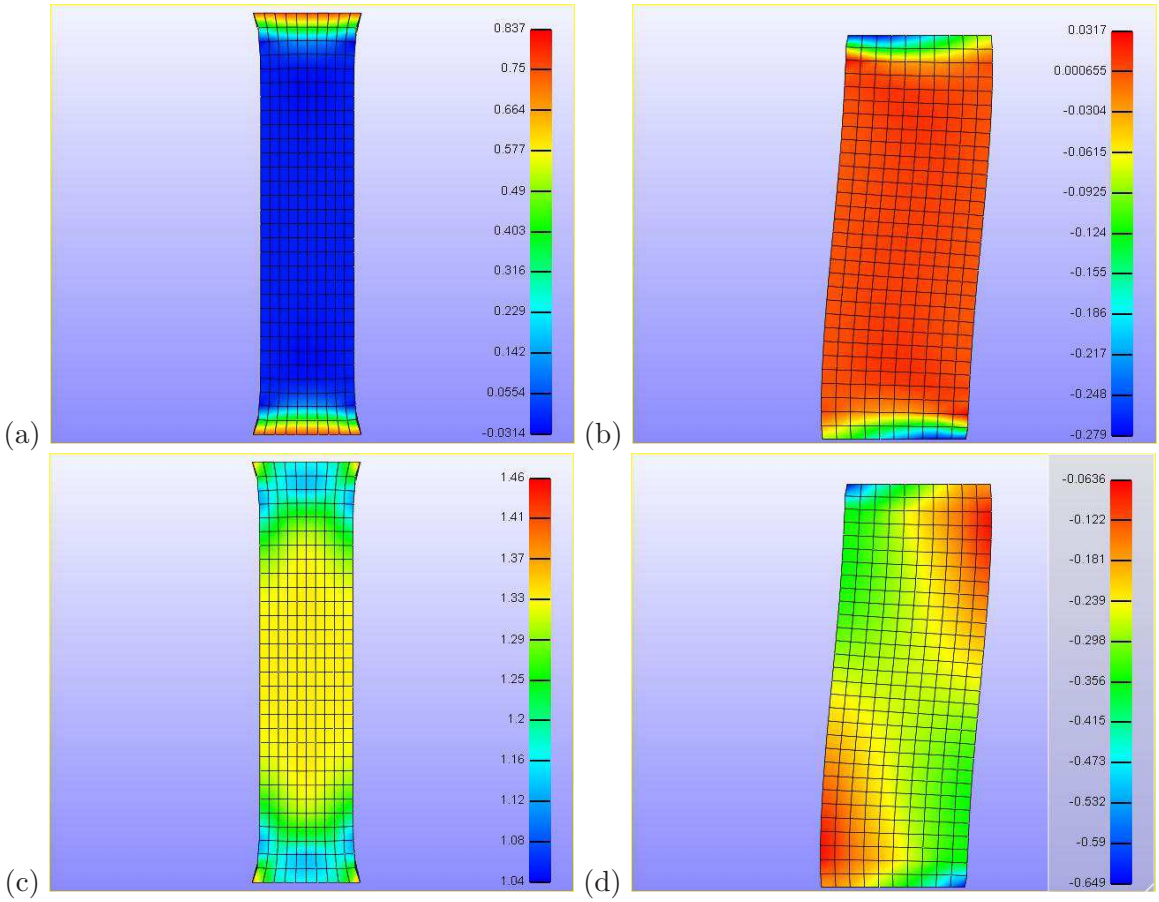

Figure 7: Deformation of a single vertical wall, showing horizontal stresses for longitudinal (a) extension and (b) compression, and vertical stresses for longitudinal (c) extension and (d) compression.

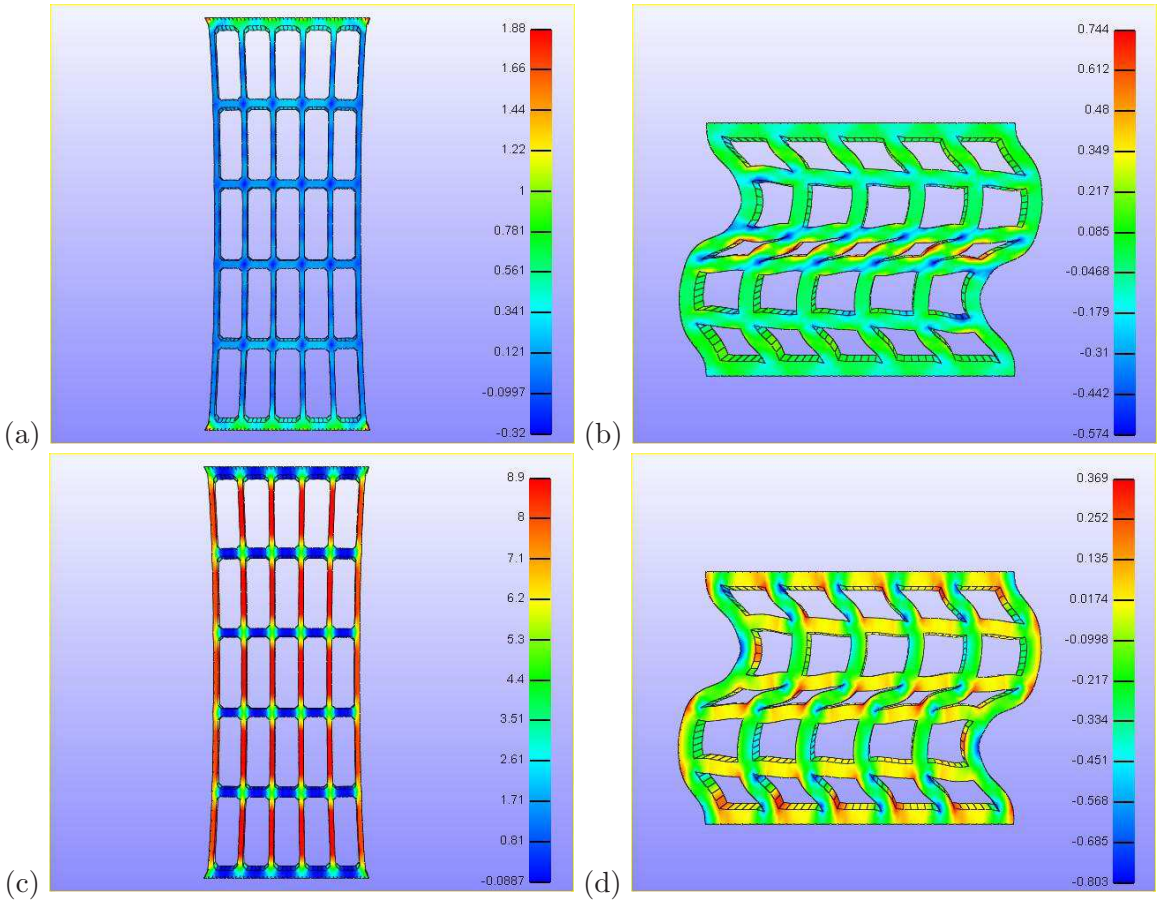

Figure 8: Deformation of cellular structure with stacked cells, showing horizontal stresses when (a) $\lambda = 2$ and (b) $\lambda = 0.82$, and vertical stresses when (c) $\lambda = 2$ and (d) $\lambda = 0.82$. Note that the cells in the middle horizontal row deform more than those situated above or below.

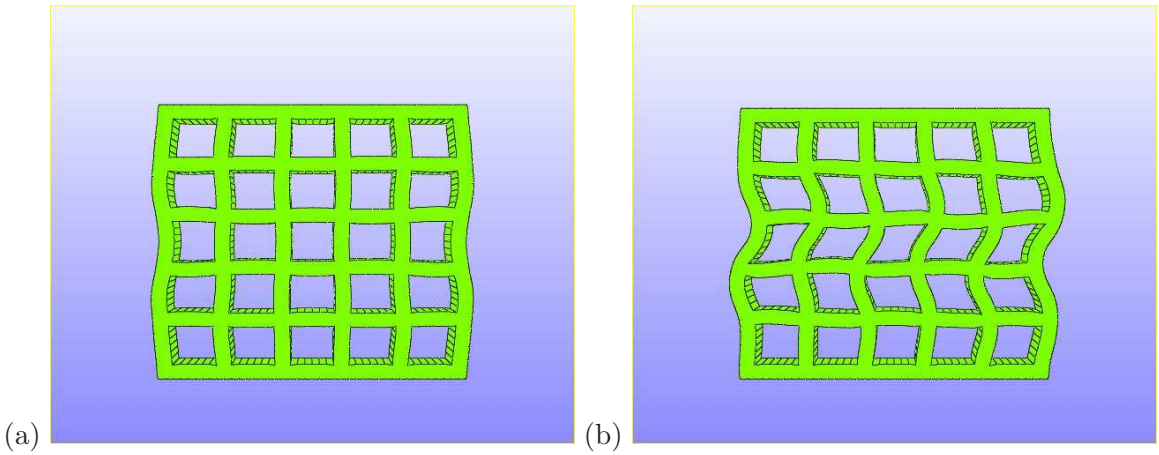

Figure 9: Deformation of cellular structure with stacked cells under compression, showing (a) the unstable symmetric solution, followed by (b) the stable buckled solution obtained by the numerical procedure.

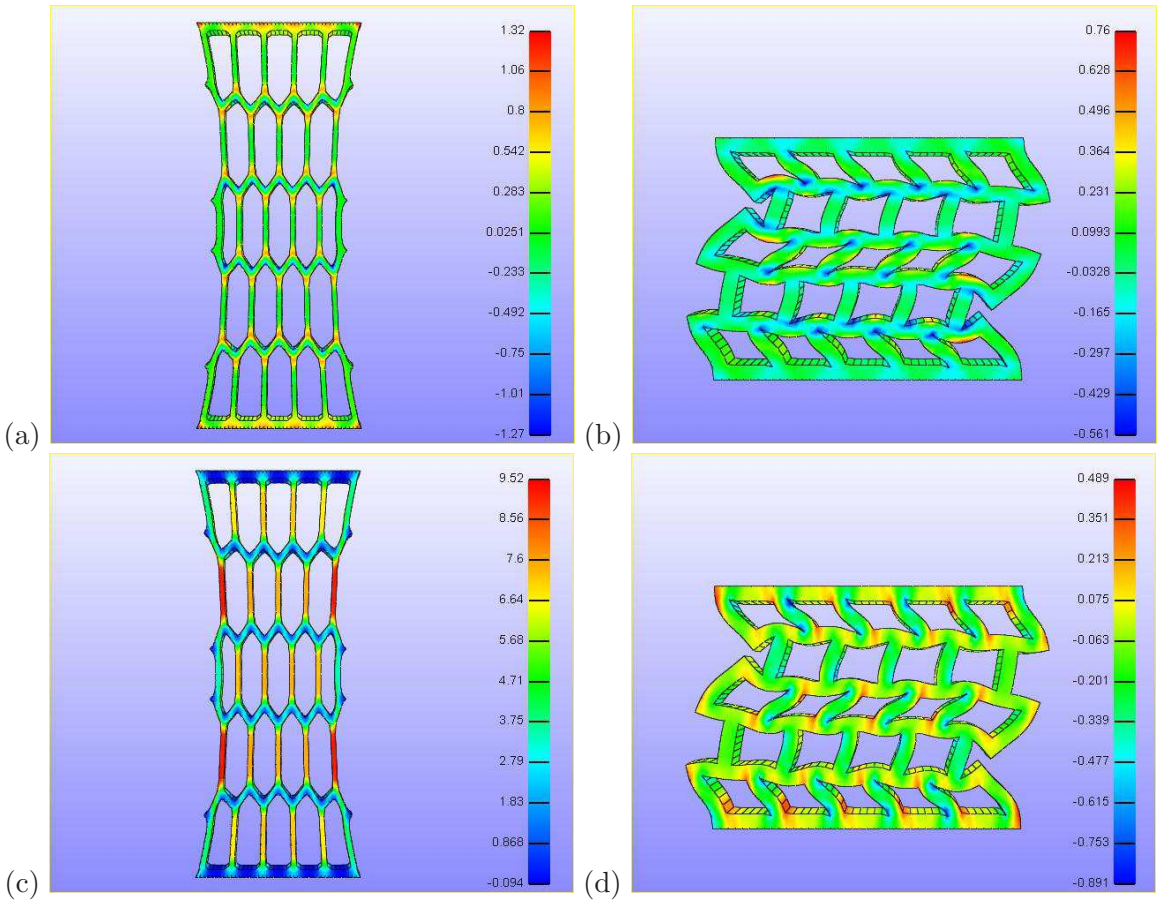

Figure 10: Deformation of cellular structure with staggered cells, showing horizontal stresses when (a) $\lambda = 2$ and (b) $\lambda = 0.82$, and vertical stresses when (c) $\lambda = 2$ and (d) $\lambda = 0.82$. In this case, the cells become hexagonal.

4 Inflation and Compression Effects in a Cellular Tube

Next, we consider a circular tube obtained by wrapping together two opposite sides of a thin rectangular section of an incompressible material wherefrom some parts were removed creating a uniform network of disconnected square cells, as illustrated in Figure 11.

(a) 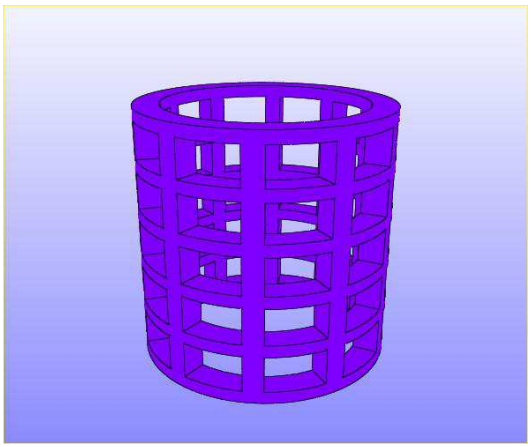 (b) 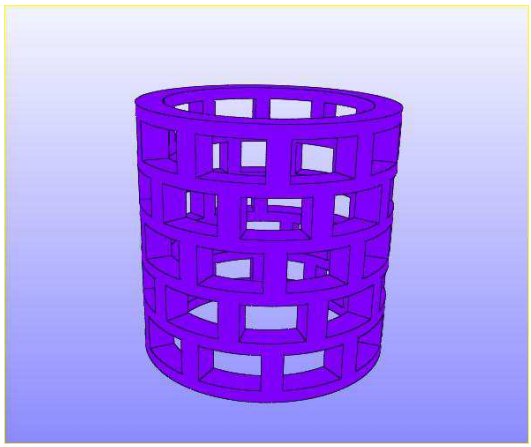

Figure 11: Undeformed cellular circular tube with (a) stacked and (b) staggered cells.

Assuming that the longitudinal axis of the tube and two sides of each cell are in the direction X_3, and the inner and outer radii are A and B, respectively, we examine the deformation of this cellular tube when its end surfaces are subject to the uniform stretch:

$$r = f(R), \qquad \theta = \Theta, \qquad z = \lambda Z, \tag{4.1}$$

where

$$f(R) = \sqrt{\frac{R^2}{\lambda} + C}, \qquad C = A^2\left(1 - \frac{1}{\lambda}\right),$$

(r, θ, z) and (R, Θ, Z) are the cylindrical coordinates for the current and undeformed configuration, respectively, and $l = \lambda L$ is the length of the tube after deformation, while all the other surfaces are free.

For the cellular tube, we identify the axial direction Z with the vertical direction, and assume that, if the tube is subject to axial tension, then extension in the longitudinal direction is accompanied by contraction in the cross-sectional directions (deflation), and if the tube is subject to axial compression, then contraction in the longitudinal direction is accompanied by expansion in the cross-sectional directions (inflation) (see Section 2.2).

For the deformation of this cellular tube, we apply the same SDP as in the case of a cellular material under axial stretch, as discussed in Section 3. Specifically, we decompose the deformation of the tube as follows:

(i) A deformation (4.1), and

(ii) A deformation where the traction constraints at the cell walls are removed, while the external conditions (4.1) at the ends of the tube are maintained.

At step (i), the deformation gradient in the cylindrical coordinate system (R, Θ, Z) is:

$$\mathbf{F}' = \begin{bmatrix} f'(R) & 0 & 0 \\ 0 & f(R)/R & 0 \\ 0 & 0 & \lambda \end{bmatrix} = \begin{bmatrix} R/\left(\lambda\sqrt{(1/\lambda)R^2 + C}\right) & 0 & 0 \\ 0 & \sqrt{(1/\lambda)R^2 + C}/R & 0 \\ 0 & 0 & \lambda \end{bmatrix},$$

and the non-zero components of the Cauchy stress tensor take the form (2.8) [30, p. 190]:

$$\begin{aligned}
\sigma_{rr} &= -\int \left(\frac{1}{\lambda}\beta_1 - \lambda\beta_{-1}\right)\left(\frac{r^2-C}{r^3} - \frac{r}{r^2-C}\right) dr, \\
\sigma_{\theta\theta} &= \sigma_{rr} - \left(\frac{1}{\lambda}\beta_1 - \lambda\beta_{-1}\right)\left(\frac{r^2-C}{r^2} - \frac{r^2}{r^2-C}\right), \\
\sigma_{zz} &= \sigma_{rr} - \frac{1}{\lambda}\left(\frac{r^2-C}{r^2} - \lambda^3\right)\beta_1 + \lambda\left(\frac{1}{\lambda^3} - \frac{r^2}{r^2-C}\right)\beta_{-1}.
\end{aligned}$$

Remark 4.1 *Note that, although the deformation (4.1) is non-affine, since the corresponding Cauchy stress depends only on r, this deformations is still compatible with the response of an isotropic homogeneous elastic body [30, pp. 184-186].*

For an axial elongation ($\lambda > 1$):

(i) At the first step of the SDP, the cellular tube deforms by the longitudinal extension (4.1). Since $C > 0$, setting $\sigma_{rr} = 0$ at $r = B$ implies $\sigma_{rr} < 0$ for all $r < B$, *i.e.* when the outside surface is free, there is internal compression acting in the radial direction. Similarly, setting $\sigma_{rr} = 0$ at $r = A$ implies $\sigma_{rr} > 0$ for all $r > A$, *i.e.* when the inside surface is free, there is external tension acting in the radial direction.

(ii) At the second step, for a pre-deformed vertical wall, the boundary conditions (2.7) are maintained at the ends while the vertical sides are set free. Assuming that the wall is long and thin, as for a vertical wall of the cellular structures discussed in Section 3, extension in the longitudinal (vertical) direction is accompanied by compression in the cross-sectional directions.

For a pre-deformed transverse wall, when the side surfaces are set free, due to the stresses for the homogeneous deformation described at step (i), this wall will contract in the circumferential direction. Then, by a similar argument as in Section 3, the vertical walls which intersect the transverse wall will bend towards the longitudinal axis. Consequently, the pre-deformed structure will contract non-uniformly in the cross-sectional directions, with the maximum contraction along the cross-sectional plane of symmetry.

For an axial contraction ($\lambda < 1$):

(i) In the first step of the SDP, the cellular tube is deformed by the longitudinal contraction (4.1). Since $C < 0$, setting $\sigma_{rr} = 0$ at $r = B$ implies $\sigma_{rr} > 0$ for all $r < B$, *i.e.* when the outside surface is free, there is internal tension in the radial direction. Similarly, setting $\sigma_{rr} = 0$ at $r = A$ implies $\sigma_{rr} < 0$ for all $r > A$, *i.e.* when the inside surface is free, there is external compression acting in the radial direction.

(ii) In the second step, for a pre-compressed vertical wall, the boundary conditions (4.1) are maintained at the ends, and if the sides of the wall are set free, then the wall will expand in the cross-sectional directions, buckle, or bend.

For a pre-compressed transverse wall, when the surface constraints derived from the homogeneous stress at step (i) are removed, the wall may expand in the radial direction (barreling).

At the structural level, when the cellular tube is compressed in the longitudinal direction and all the surface constraints at the pre-deformed cell walls are removed, the pre-deformed cellular material will tend to expand in the radial direction. In this case, stable deformations which are symmetric with respect to the longitudinal axis are possible (barrelling), as well as asymmetric deformations (buckling).

In the linear elastic limit $\lambda \to 1$, the deformation of the cellular tube is almost uniform.

4.1 Extension or Compression of a Cellular Tube of Mooney Material

For a cellular circular tube of Mooney material (3.3), which is either extended or compressed in the axial direction, the deformation and stresses are illustrated in Figures 14 and 15, for stacked and staggered cell distribution, respectively. In Figure 14, the vertical walls bend or buckle, while the transverse walls remain horizontal, as predicted by the successive decomposition procedure. In Figure 15, due to the additional bending of the transverse walls, the cells become hexagons where the oblique walls are sheared.

For the cellular tubes, we tested also the effect of a small lateral traction acting during the longitudinal compression. For this case, the resulting buckling-like deformations are shown in Figures 12 and 13. Since a larger lateral pressure was required to obtain this deformation for the tube with staggered cells than for the tube with stacked cells, we infer that the barrelling deformation is more stable for structures with staggered cells than for the stacked cell structures.

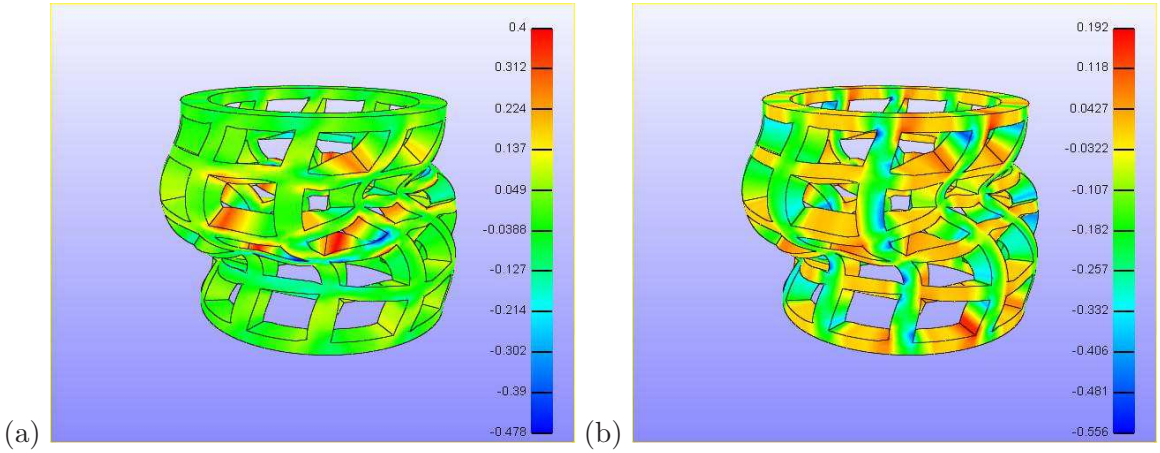

Figure 12: Longitudinal compression with small lateral pressure for cellular tube with stacked cells, showing (a) horizontal and (b) vertical stresses.

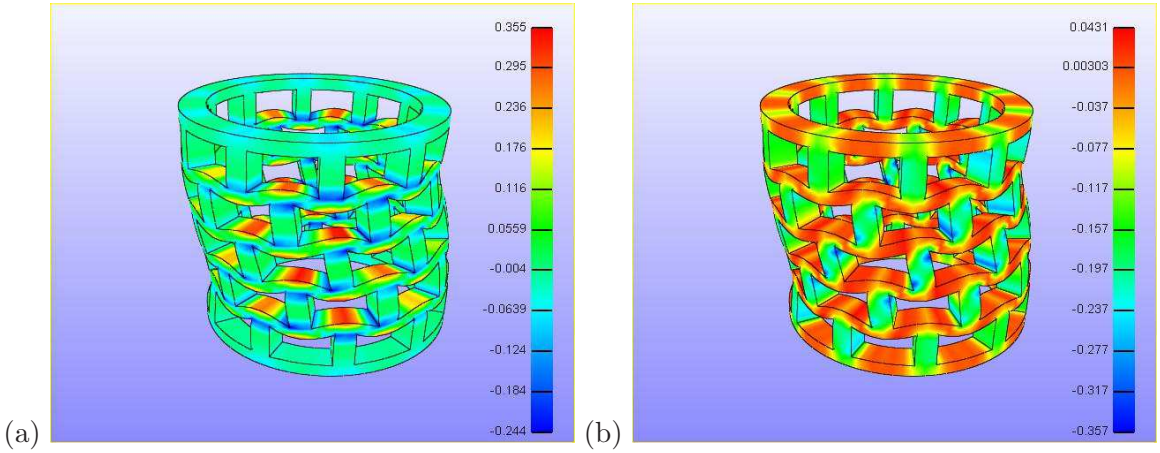

Figure 13: Longitudinal compression with small lateral pressure for cellular tube with staggered cells, showing (a) horizontal and (b) vertical stresses.

When the tube is extended axially, the resulting non-uniform deformation is due to the fact that, when the side surfaces of the tube deform freely, the radius of each cross-section decreases, causing the vertical walls which are held fixed at the ends to bend.

In axial compression, for a compact circular cylinder of a neo-Hookean material, both axisymmetric (barrelling) and asymmetric (buckling) deformation modes were shown to occur [11], whereas only asymmetric buckling deformations are captured by linear elastic models. When we tested numerically

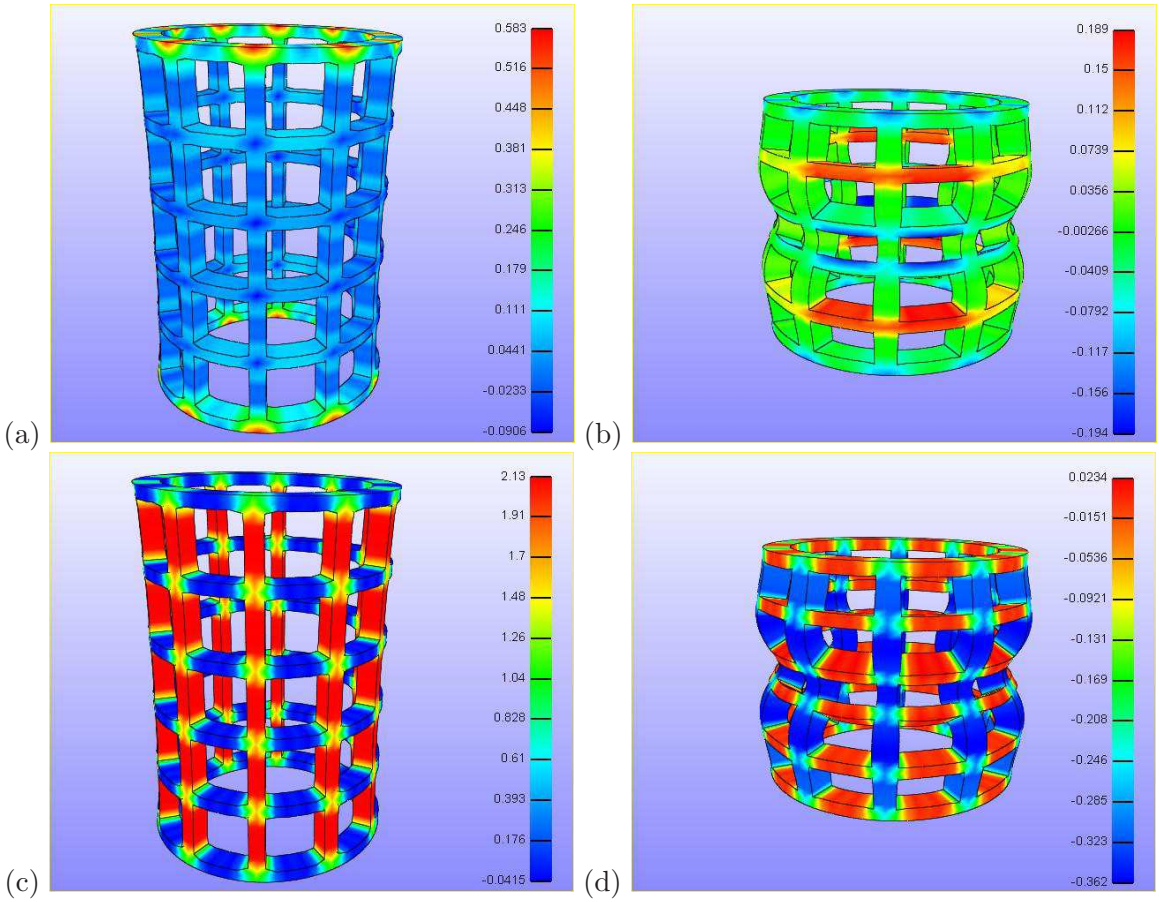

Figure 14: Axisymmetric deformation of cellular tube with stacked cells, showing horizontal stresses when (a) $\lambda = 1.5$ and (b) $\lambda = 0.8$, and vertical stresses when (c) $\lambda = 1.5$ and (d) $\lambda = 0.8$. Note that the cells in the middle horizontal row deform more than those situated above or below.

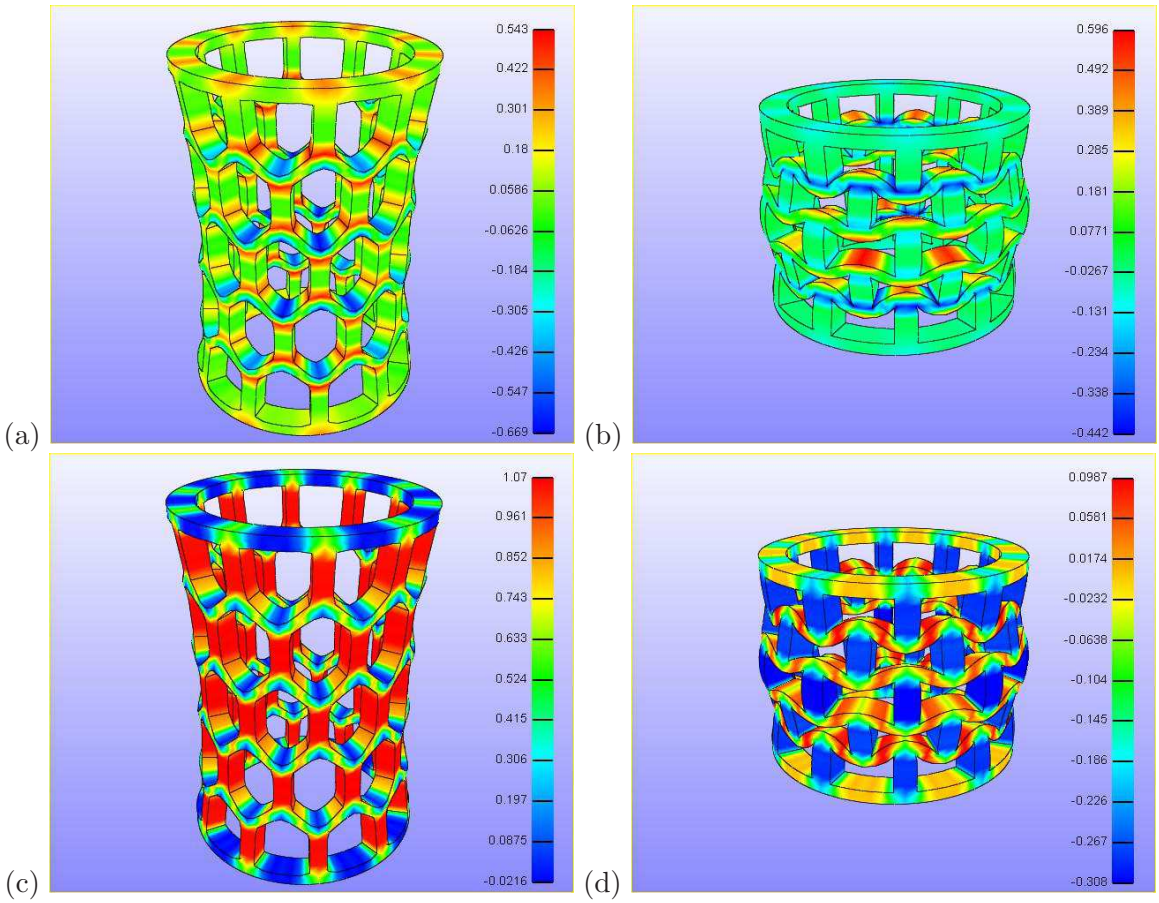

Figure 15: Axisymmetric deformation of cellular tube with staggered cells, showing horizontal stresses when (a) $\lambda = 1.5$ and (b) $\lambda = 0.8$, and vertical stresses when (c) $\lambda = 1.5$ and (d) $\lambda = 0.8$. For this tube, the cells become hexagonal.

the mechanical behaviour of cellular tubes made of a linearly elastic material, we found that, unlike for the compact tube, barreling solutions are possible under longitudinal compression.

5 Shearing Responses in a Cellular Structure (or How to Avert Collapse)

We also investigate the deformation of the thin cellular structure introduced Section 3, when two opposite external faces are subject to the simple shear conditions (2.9), while the other surfaces are free.

We decompose this deformation as follows:

(i) We start with the (homogeneous) simple shear (SS) deformation (2.9) everywhere in the structure.

(ii) Then, we set the cell walls free by removing the traction constraints at the walls, while the SS conditions are maintained on the external sheared boundaries.

Remark 5.1 *Following the analysis in Section 2.3), for the hyperelastic cell walls, two cases are distinguished: (i) $\beta_{-1} < 0$, which leads to a positive Poynting effect in a hyperelastic material subject to shear, and (ii) $\beta_{-1} > 0$, leading to a negative Poynting effect.*

For a positive Poynting effect in the cell wall material ($\beta_{-1} < 0$):

(i) At the first step of the SDP, where the simple shear (2.9) is assumed everywhere in the structure, for an initially vertical or horizontal cell wall, the surface tractions (2.10) and (2.11) are active. Hence these walls are compressed in the directions normal to their surfaces and sheared in the tangential directions.

If $\mathbf{v}_1$ and $\mathbf{v}_2$ are the principal directions for the simple shear deformation, then every cell wall is extended in the $\mathbf{v}_1$ direction and compressed in the $\mathbf{v}_2$ direction. Moreover, since $\sigma_1 - \sigma_2 = (\beta_1 - \beta_{-1})K\sqrt{K^2+4} > 0$, for large values of K, the structure extends mainly in the direction of its lengthening diagonal.

(ii) At the second step, for a pre-sheared vertical wall, if the ends remain sheared and the (inclined) sides are set free, then the remaining tractions are $\sigma_n = \sigma_{22} < 0$ and $\sigma_t = -\sigma_{12} < 0$ at the ends. Translating the end tractions into axial and transverse loads for this wall yields:

$$\sigma_N = \frac{\sigma_{22}}{\sqrt{1+K^2}} + \frac{K\sigma_{12}}{\sqrt{1+K^2}} = \frac{\beta_1 K^2}{\sqrt{1+K^2}} > 0,$$
$$\sigma_T = \frac{K\sigma_{22}}{\sqrt{1+K^2}} - \frac{\sigma_{12}}{\sqrt{1+K^2}} = \frac{\beta_{-1}K^3 - (\beta_1 - \beta_{-1})K}{\sqrt{1+K^2}} < 0,$$

hence this wall will bend.

If $\mathbf{v}_1$ and $\mathbf{v}_2$ are the principal directions from step (i), as the sides deform freely, a pre-sheared vertical wall will tend to contract in the direction $\mathbf{v}_1$, but since its ends are fixed, the wall will mainly stretch in this direction, and will extend in the $\mathbf{v}_2$ direction also. Due to the fixed ends of the wall, a contraction in the $\mathbf{v}_1$ direction will also take place near the ends of its 'shortening diagonal'.

For a pre-sheared horizontal wall, when all traction constraints are removed, the wall will tend to expand in the directions normal to its surfaces [30, p. 183]. Also, a pre-sheared horizontal wall will contract in the direction $\mathbf{v}_1$ and expand in the direction $\mathbf{v}_2$, causing the initially vertical walls to bend.

Thus the pre-deformed cellular material will expand in the direction $\mathbf{v}_2$, and due to the bending of the originally vertical walls, the deformation will be non-uniform.

For a negative Poynting effect in the cell wall material ($\beta_1 > \beta_{-1} > 0$):

(i) In the first step of the SDP, the simple shear (2.9) is assumed throughout the structure, while the shear parameter K satisfies (2.18).

(ii) In the second step, due to the tension compression behaviour in the $\mathbf{v}_1$ and $\mathbf{v}_2$ directions, the pre-sheared material will behave similarly to the case when $\beta_{-1} < 0$. However, the lower amount of shear allowed in a material capable of exhibiting the negative Poynting effect may preclude cell closure.

In the linear elastic limit $K \to 0$, under the simple shear deformation the inclined sides are stress free, and the shear deformation of the cellular structure is equivalent to a simple shear.

5.1 Shearing Effects in a Cellular Structure of Mooney Material

When a solid body of Mooney material (3.3) is subject to the simple shear (2.9), if $\mu_1 + 2\mu_2 < 0$, then

$$\sigma_{22} = -\frac{\mu_1 + 2\mu_2}{3} K^2 > 0,$$

i.e. the negative Poynting effect occurs. Also:

$$\beta_0 = \frac{(\mu_2 - \mu_1)(K^2 + 3)}{3}, \qquad \beta_1 = \mu_1, \qquad \beta_{-1} = -\mu_2, \tag{5.1}$$

and GEI (2.17) are valid. Under these conditions, $\sigma_{33} = (\mu_2 - \mu_1)k^2/3 < 0$, *i.e.* the stress in the direction normal to the plane of shear is compressive, and the normal traction on the inclined faces is:

$$\sigma_n = -\frac{K^4(\mu_1 + 2\mu_2) + K^2(4\mu_1 + 5\mu_2)}{3},$$

and there exists a shear parameter:

$$K_0 = \sqrt{-\frac{4\mu_1 + 5\mu_2}{\mu_1 + 2\mu_2}}, \tag{5.2}$$

such that $\sigma_n = 0$ [22].

Alternatively, if $\mu_1 + 2\mu_2 > 0$, then the positive Poynting effect is obtained. In this case, $\sigma_{33} \leq 0$ and $\sigma_n < 0$.

In our computations, for the material exhibiting the positive Poynting effect, the constitutive parameters are $\mu_1 = 1.2$ MPa, $\mu_2 = 0.2$ MPa and $\kappa = 100$ MPa (model 1), while for the material where the negative Poynting effect occurs, the constitutive parameters are $\mu_1 = 1.2$ MPa, $\mu_2 = -0.7$ MPa, and $\kappa = 100$ MPa (model 2).

In the incompressible case, by setting $\sigma_{33} = 0$, or equivalently $p = \mu_1 - \mu_2$, we obtain:

$$\sigma_{22} = -\mu_2 K^2.$$

In this case, the positive Poynting effect occurs if $\mu_2 > 0$, and the negative Poynting effect is observed if $\mu_2 < 0$ [22]. When $\mu_1 > 0$ and $\mu_2 < 0$, by (2.18), the acceptable values for the shear parameter are $K < K_c$, where $K_c = (\mu_1 + \mu_2)/\sqrt{-\mu_1\mu_2}$. In particular, if $\mu_1 = 1.2$ MPa, $\mu_2 = -0.7$ MPa, then $K < K_c = 0.5455$, and on the inclined faces, the normal traction satisfies $\sigma_n > 0$ for all $K > 0$.

For the numerical simulations, we first consider an elastic cell wall of size $1 \times 3 \times 1$, formed from either material model 1 or 2, and subject to various boundary conditions relevant in a cellular structure deformed under external shear. In the graphical representations of the deformed cell wall, the finite element mesh is also shown.

In Figure 16, the deformation and vertical stresses in the cell wall with SS conditions (2.9) at the ends and zero vertical displacement on the inclined faces are illustrated. For the wall made of material model 1, the vertical stress throughout the wall is compressive, Figure 16 (a), while for material model 2, the vertical stress is tensile, Figure 16 (b). However, in both cases, the first principal stress is tensile and the second principal stress is compressive, as seen in Figure 17.

For a single cell wall made of either material model 1 or 2, the deformed configuration and principal stresses when the ends are subject to SS conditions and the side faces are free are represented in

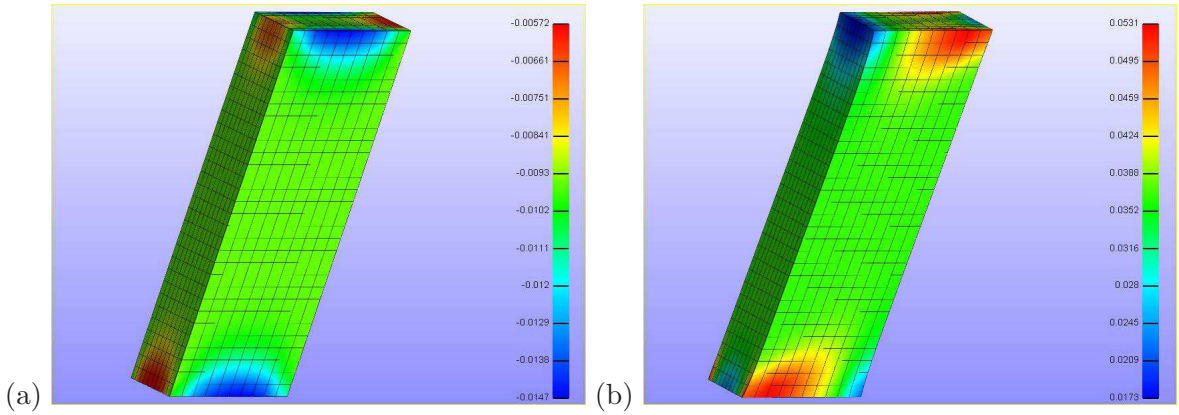

Figure 16: Deformation of vertical cell wall with SS conditions at the ends and zero vertical displacement on the inclined faces, showing vertical stresses: (a) compressive for model 1, (b) tensile for model 2.

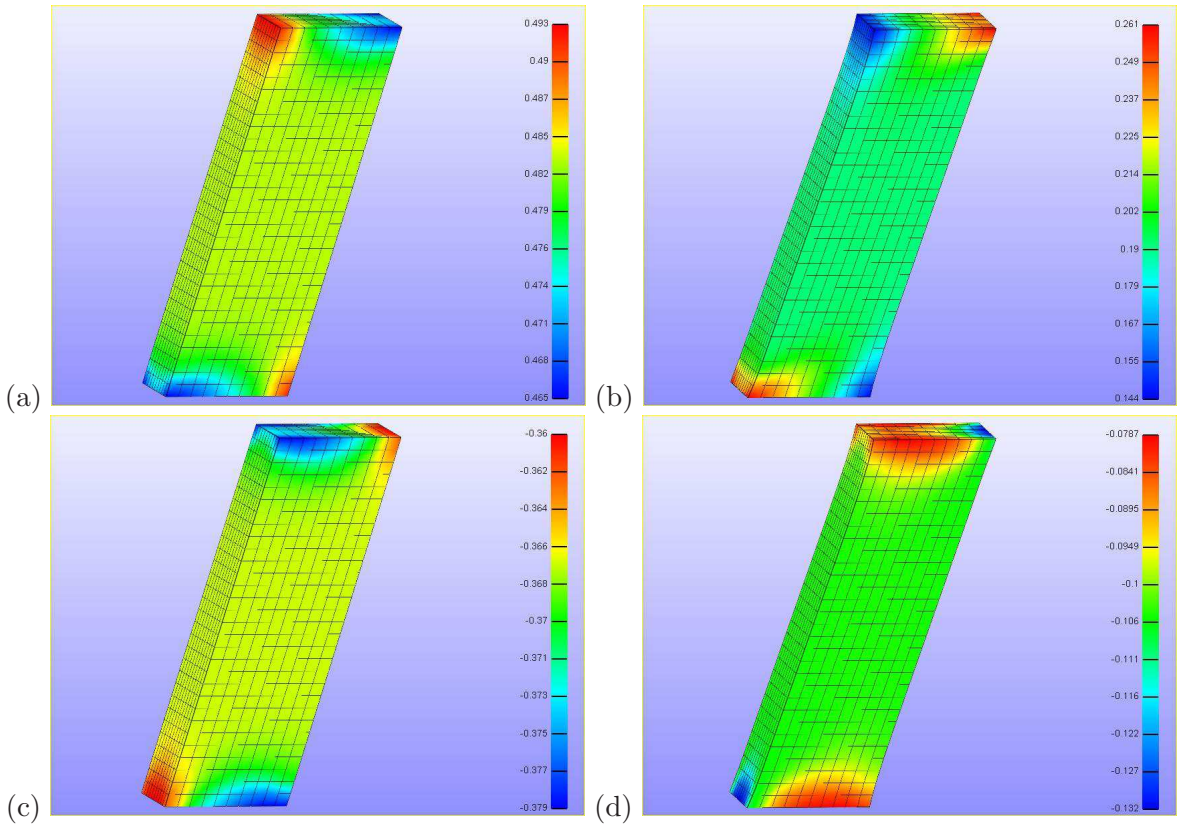

Figure 17: Deformation of vertical cell wall with SS conditions at the ends and zero vertical displacement on the inclined faces, showing first principal stresses for (a) model 1 and (b) model 2, and second principal stresses for (c) model 1 and (d) model 2.

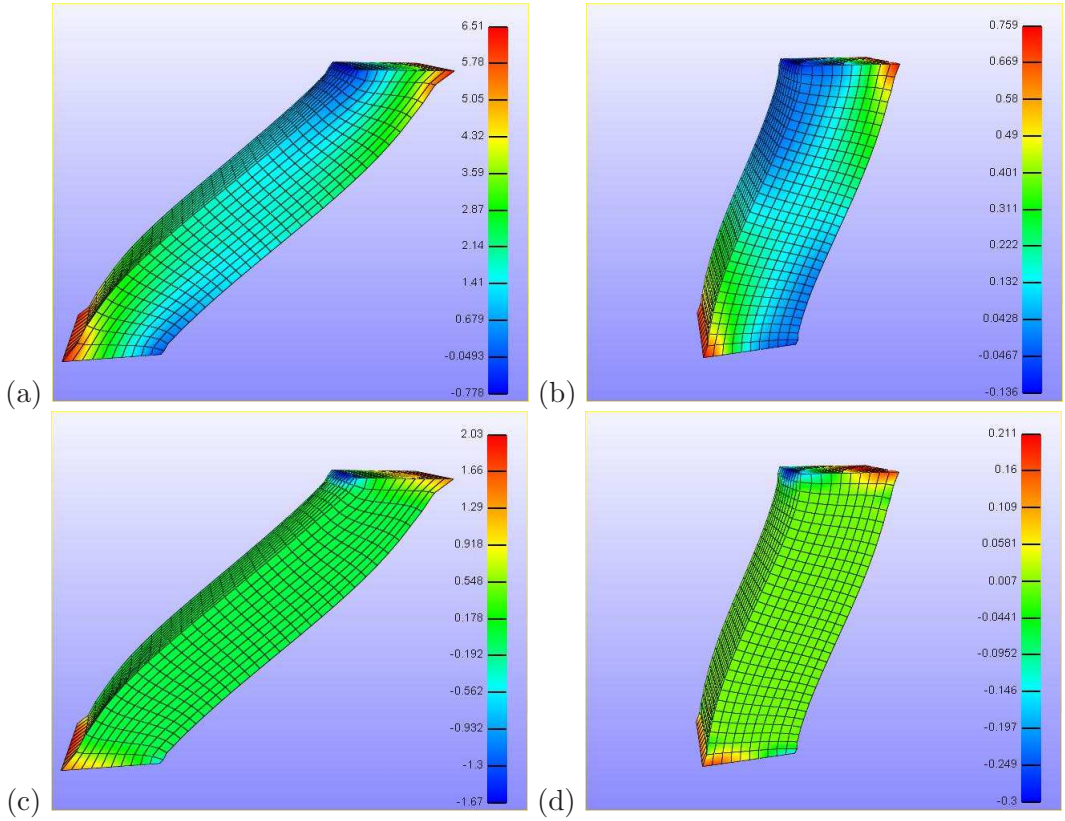

Figure 18: Deformation of vertical cell wall with SS conditions at the ends, showing first principal stresses for (a) model 1 and (b) model 2, and second principal stresses for (c) model 1 and (d) model 2.

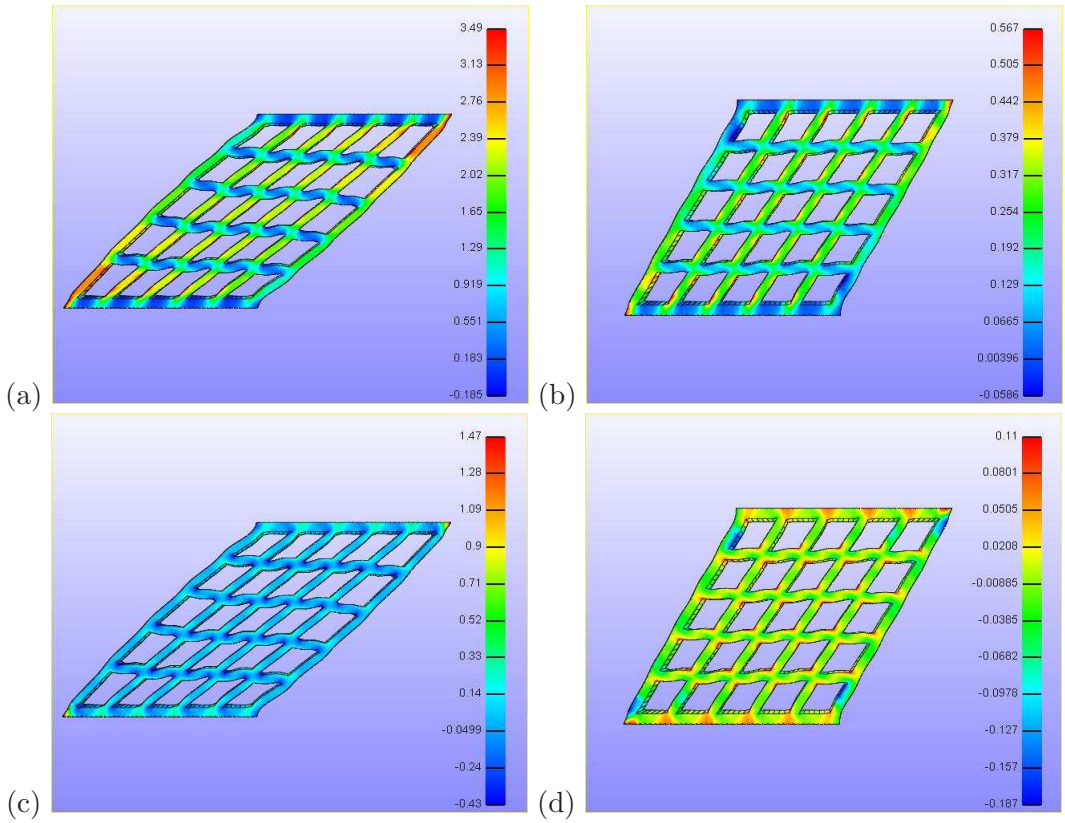

Figure 19: Deformation of cellular structure with stacked cells and two opposite faces subject to SS conditions, showing first principal stresses for (a) model 1 and (b) model 2, and second principal stresses for (c) model 1 and (d) model 2. For model 1, there is non-uniform extension in the direction of the inclined walls and also expansion in the transverse direction; for model 2, the deformation is almost uniform.

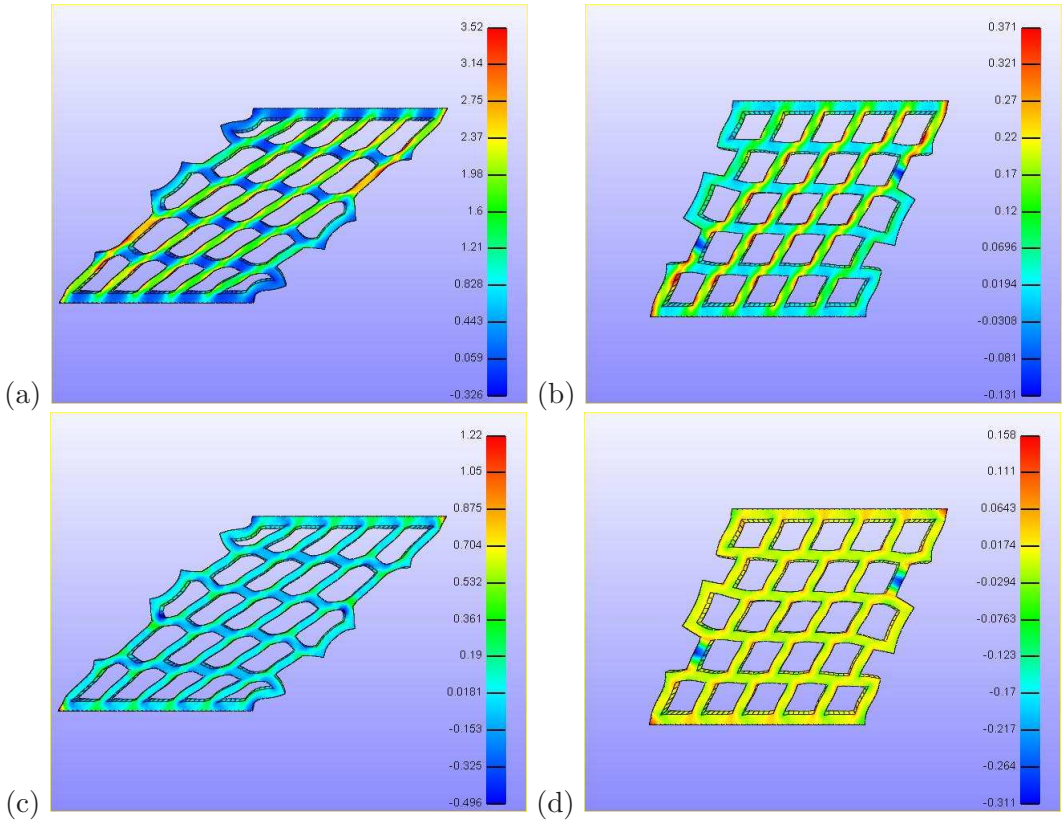

Figure 20: Deformation of cellular structure with staggered cells and two opposite faces subject to SS conditions, showing first principal stresses for (a) model 1 and (b) model 2, and second principal stresses for (c) model 1 and (d) model 2. In this case, for model 1, the cells become hexagonal.

Figure 18. In this case, the wall deforms in the same manner for the two constitutive models, except that the wall made of material model 1 is able to shear further than that formed from material model 2.

Next, we take a thin square section of a cellular structure with two opposite external faces subject to SS conditions and the other faces deforming freely. In this case, the contour of the cell walls is represented, while the finite element mesh for the individual cell walls is omitted.

For a cellular section with stacked or staggered cells made of material model 1, the deformation and principal stresses are indicated in Figures 19-20, (a) and (c), respectively. In these figures, the cells generally elongate in directions parallel to the inclined sides, and compress in the transverse directions. However, unlike in a uniform deformation, this compression decreases as the distance to one of the sides decreases, and the structure tends to expand laterally. In addition, for the structure with staggered cells, the cells assume hexagonal shapes.

For model 2, the deformation is almost uniform, as shown in Figures 19-20, (b) and (d), respectively.

6 Torsion Responses in a Cellular Tube

Next, we take a cellular circular tube with inner and outer radii A and B, respectively, and assume, as before, that the longitudinal axis of the tube and two sides of each cell are in the direction X_3 (see Figure 11). For this cellular tube, we examine the deformation where the end faces are subject to the simple torsion conditions (2.19), while the other surfaces deform freely.

To examine the behaviour of this cellular tube, we decompose its deformation as follows:

(i) A simple torsion (ST) (2.19), and

(ii) A deformation where the traction constraints at the cell walls are removed, while the ST conditions at the ends of the tube are maintained.

When the entire tube is deformed by simple torsion, the non-zero entries of the Cauchy stress tensor are as follows [30, p. 191]:

$$\sigma_{rr} = \tau^2 \int r\beta_1 dr, \qquad \sigma_{\theta\theta} = \sigma_{rr} + \tau^2 r^2 \beta_1,$$
$$\sigma_{zz} = \sigma_{rr} + \tau^2 r^2 \beta_{-1}, \qquad \sigma_{\theta z} = \tau r(\beta_1 - \beta_{-1}),$$

and depend on r only, hence are compatible with the response in an isotropic homogeneous elastic body [30, pp. 184-186].

Then setting $\sigma_{rr} = 0$ at $r = B$ implies $\sigma_{rr} < 0$ for all $r < B$, *i.e.* when the outside surface is free, there is internal compression acting in the radial direction. Similarly, setting $\sigma_{rr} = 0$ at $r = A$ implies $\sigma_{rr} > 0$ for all $r > A$, *i.e.* if the inside surface is free, then there is external tension acting in the radial direction.

Furthermore, assuming $\sigma_{rr} = 0$, if $\beta_{-1} < 0$, then $\sigma_{zz} < 0$, *i.e.* the positive Poynting effect occurs, and if $\beta_{-1} > 0$, then $\sigma_{zz} > 0$, *i.e.* the negative Poynting effect is obtained. Consequently, if $\beta_{-1} < 0$ and the outside surface is free, then $\sigma_{rr} \leq 0$ and $\sigma_{zz} < 0$ everywhere in the tube, and if $\beta_{-1} > 0$ and the inside surface is free, then $\sigma_{rr} \geq 0$ and $\sigma_{zz} > 0$ everywhere.

For a positive Poynting effect in the cell wall material ($\beta_{-1} < 0$):

(i) At the first step of the SDP, where the simple torsion (2.19) is assumed everywhere, the deformation can be treated (locally) as simple shear.

(ii) At the second step, where only the ends of the tube are subject to (2.19), the deformation can be treated by analogy to the shear problem in Section 2.4.

In the absence of normal tractions at the side surfaces, on the internal surface, the pressure in the radial direction decreases, and the cross-sectional areas become smaller, causing the horizontal walls to bend.

For a negative Poynting effect in the cell wall material ($\beta_1 > \beta_{-1} > 0$):

(i) In the first step of the SDP, the simple torsion (2.19) takes place everywhere, and the deformation can be regarded locally as a simple shear.

(ii) In the second step, the deformation of these walls is similar to that for the shear problem.

For this case, in the absence of normal tractions at the side surfaces, the pressure on the external surface increases, causing a reduction in the cross-sectional area, and thus the horizontal walls will bend.

Although there are no apparent differences in the behaviour of this tube compared to that made of a material showing the positive Poynting effect, the lower amount of shear allowed in the material exhibiting the negative Poynting effect may preclude cell closure.

When $K \to 0$, the torsion of the cellular tube is almost uniform.

6.1 Twisting Effects in a Cellular Tube of Mooney Material

We examine numerically a cellular tube of Mooney material (3.3), where the end faces are subject to the ST conditions (2.19) and the side surfaces deform freely. In this case also, only the contour of the cell walls is shown in the graphical illustrations, while the finite element mesh is omitted. When a continuous tube is depicted, the corresponding finite element mesh is also shown.

(a) 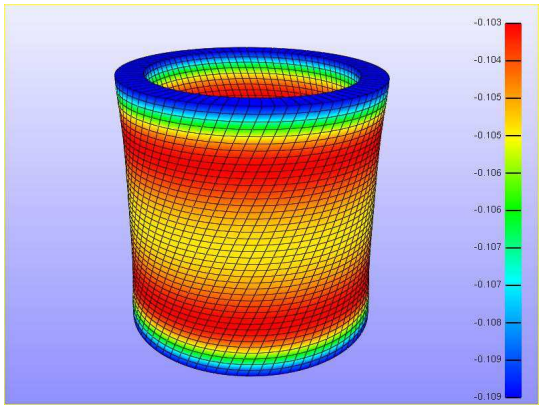

(b) 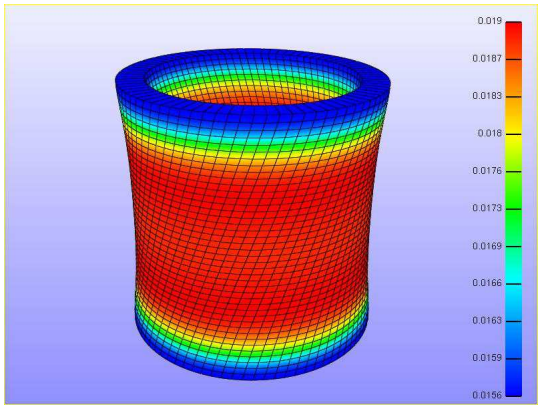

Figure 21: Deformation of vertical tube with ST conditions at the ends, showing axial stresses: (a) compressive for model 1, (b) tensile for model 2.

In view of the finite element representation, we first express the ST deformation (2.19) equivalently in rectangular (Cartesian) coordinates to obtain [22]:

$$\begin{aligned} x_1 &= X_1 \cos(\tau X_3) + X_2 \sin(\tau X_3), \\ x_2 &= -X_1 \sin(\tau X_3) + X_2 \cos(\tau X_3), \\ x_3 &= X_3. \end{aligned}$$

In this form, the deformation gradient is:

$$\mathbf{F} = \begin{bmatrix} \cos(\tau X_3) & \sin(\tau X_3) & -\tau X_1 \sin(\tau X_3) + \tau X_2 \cos(\tau X_3) \\ -\sin(\tau X_3) & \cos(\tau X_3) & -\tau X_1 \cos(\tau X_3) - \tau X_2 \sin(\tau X_3) \\ 0 & 0 & 1 \end{bmatrix},$$

and the strain invariants are, respectively:

$$I_1 = \tau^2(X_1^2 + X_2^2) + 3 = I_2 \qquad \text{and} \qquad I_3 = 1.$$

For the Mooney-Rivlin material, $\beta_1 = \mu_2$ and $\beta_{-1} = -\mu_2$, and after setting the hydrostatic pressure $p = \mu_1 - \mu_2$, the Cauchy stress in the X_3-direction is equal to:

$$\sigma_{33} = -\mu_2 \tau^2 (X_1^2 + X_2^2).$$

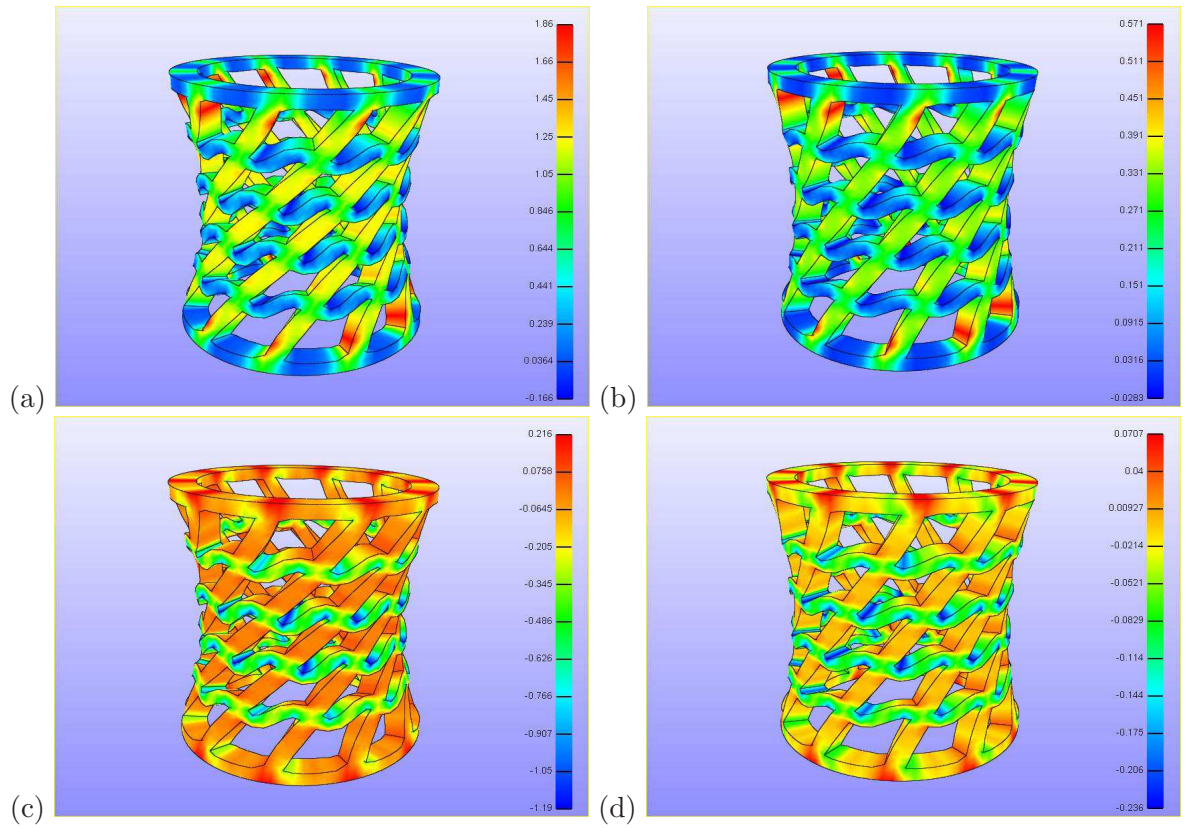

Figure 22: Deformation of cellular tube with stacked cells and ST conditions at the ends, showing first principal stresses for (a) model 1 and (b) model 2, and second principal stresses for (c) model 1 and (d) model 2. Note the contraction of the transverse walls under the shear type deformation of individual cells.

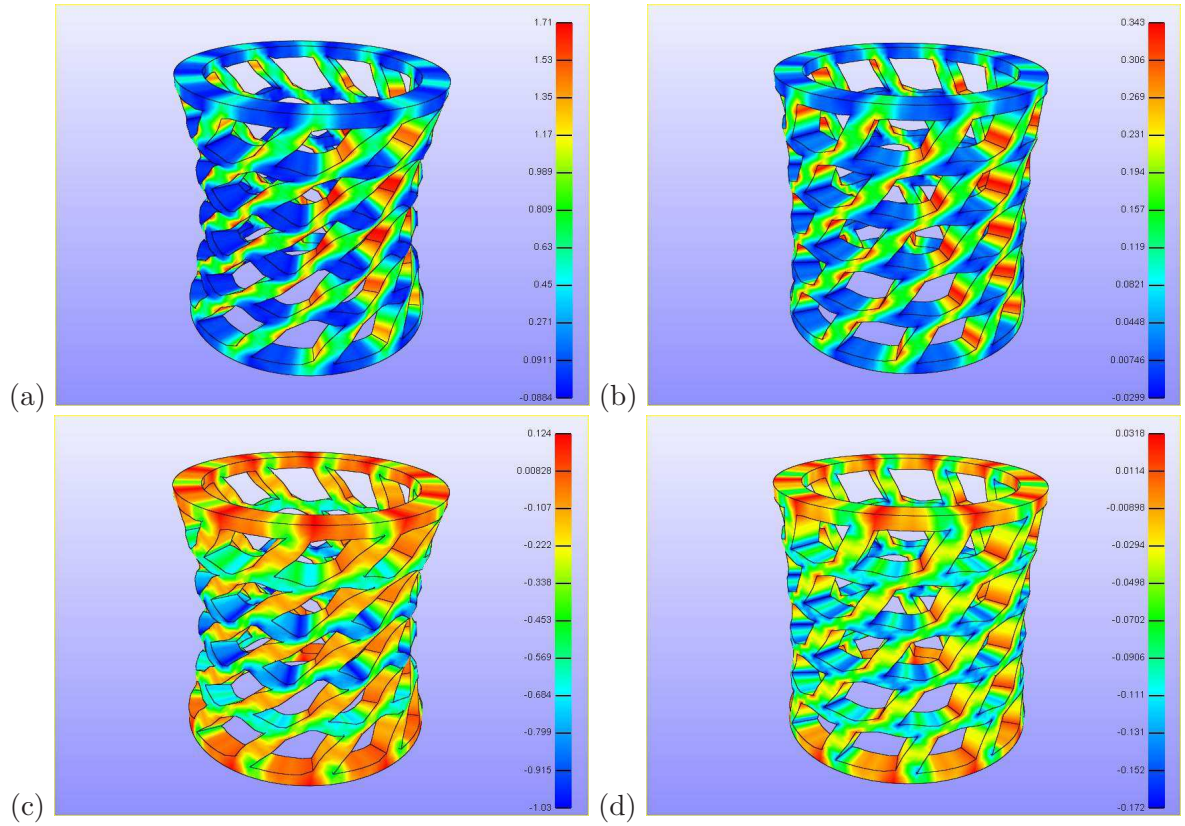

Figure 23: Deformation of cellular tube with staggered cells and ST conditions at the ends, showing first principal stresses for (a) model 1 and (b) model 2, and second principal stresses for (c) model 1 and (d) model 2. In this case, the orientation of the transverse walls also changes.

Therefore, if $\mu_2 > 0$, then $\sigma_{33} < 0$, corresponding to the positive Poynting effect, and if $\mu_2 < 0$, then $\sigma_{33} > 0$, showing the opposite sign effect.

In Figure 21, the vertical stresses which are compressive for a compact tube made of material model 1 and tensile for the tube made of material model 2, are indicated. However, this difference only precludes very large local deformations in the material model 2, and does not affect the manner by which the cellular tubes will deform under similar external conditions.

For cellular tubes with either stacked or staggered cells made of material model 1, the deformation and principal stresses are illustrated in Figures 22-23 (a) and (c), respectively. In both cases, the cells near the central cross-section are smaller than those above or below, with the cells at the ends of the tube being the largest. This non-uniform deformation is due to the fact that, when the side surfaces of the tube deform freely, the cross-sectional area decreases.

For tubes made of material model 2, the similar deformation and stresses are represented in Figures 22-23 (b) and (d), respectively. However, in this case, there is a smaller amount of shear for the individual cells.

7 Mitigating Cell Closure: The Effects of Cell Wall Heterogeneity

Many natural cellular structures maintain their integrity under unforeseen or more typical loading conditions by adjusting their composition or quantity in responses to changes in loads through a combination of fibre reinforcement or thickening of the walls in load-bearing regions [10, 25]. In this section, we analyse the mechanical behaviour of the cellular structures introduced earlier when the cell walls are made of fibre composite material, and also when the architecture of the structure changes by increasing the wall thickness in selected regions.

7.1 Increased Cell Wall Thickness in Selected Regions

We consider cellular structures with stacked and staggered cells where the cell walls along the middle horizontal row are thicker than the other walls (see Figure 24). The middle row was chosen since, in our previous models with uniform cell walls, this row appeared to suffer the largest deformations under symmetric loading conditions.

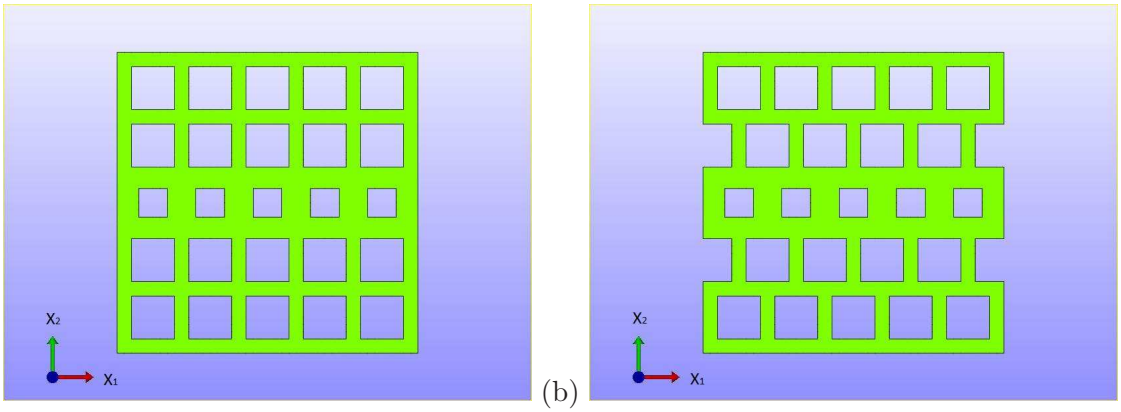

Figure 24: Undeformed square section of cellular material with (a) stacked and (b) staggered cells, and thicker cell walls in the middle row.

When the structures with thicker cell walls are subject to uniaxial tension, there are no significant differences in the incurred deformation from those with uniform walls, as seen from Figure 25. However, under compression, the deformation for the modified structure is more likely to be axisymmetric, as shown in Figure 26.

(a) 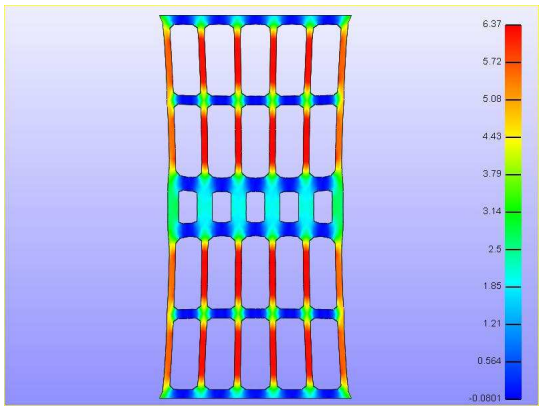

(b) 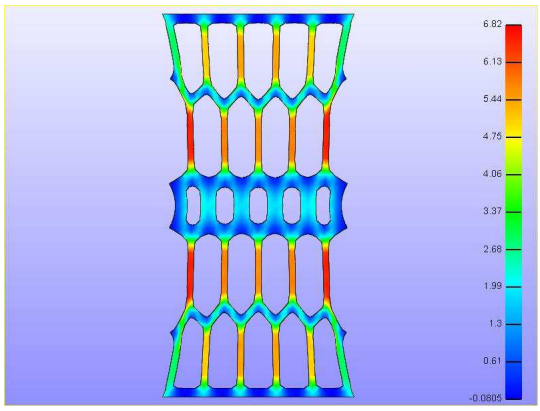

Figure 25: Vertical extension and stresses in cellular structure with (a) stacked and (b) staggered cells, and thicker cell walls in the middle row.

(a) 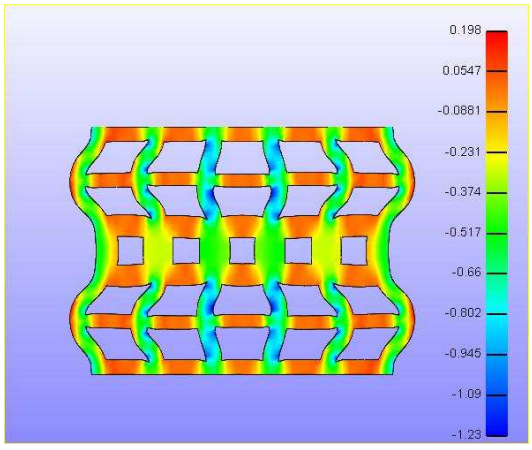

(b) 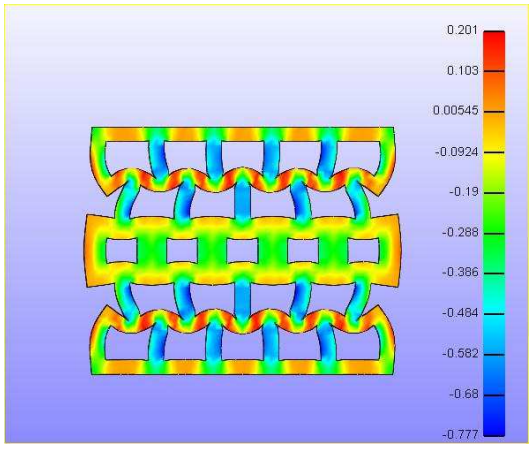

Figure 26: Vertical compression and stresses in cellular structure with (a) stacked and (b) staggered cells, and thicker cell walls in the middle row.

7.2 Fibre Reinforced Cell Walls

Assuming that the cell wall material is a fibre reinforced composite, we investigate the effects of fibre reinforcement at the structural level. Mechanically speaking, fibres are one dimensional bodies whose performance is determined by their longitudinal strength and stiffness. Like the cellular structure itself, fibres are strong in tension, not in compression, but their lay-out is important as it accounts for part of the great overall anisotropy of the composite. In many structural materials (e.g. marine sponge, plant stems), the fibre direction is nearer the cell axis than across it, and one can assume the fibres to align with the longitudinal direction of the walls.

If a fibre oriented along the unit vector $\mathbf{M}$ in the reference configuration can stretch and is subject to a deformation with deformation gradient $\mathbf{F}$, then the stretch of the fibre λ_m is given by the parameter $I_m = \lambda_m^2 = \mathbf{M}^T\mathbf{C}\mathbf{M}$. Let $W_m^{fb}(I_m)$ be the stored energy density of the fibre, then the Cauchy stress for the fibre is:

$$\boldsymbol{\sigma}^{fb} = 2J^{-1}I_m\frac{\partial W_m^{fb}}{\partial I_m}\mathbf{m}\otimes\mathbf{m},$$

where $\mathbf{m} = \mathbf{F}\mathbf{M}/\lambda_m$ is the unit vector for the orientation of the fibre in the current configuration and $J = \det\mathbf{F}$. Since a fibre can sustain tension but not compression, its stress tensor is pre-multiplied by $H(I_m - 1)$, where $H(\cdot)$ is the Heaviside (or unit step) function.

In the numerical examples, we assume that the fibres are embedded in a Mooney-Rivlin material, and the resulting cell wall material is described by the hyperelastic strain energy function:

$$\mathcal{W} = \frac{\mu_1}{2}\left(I_3^{-1/3}I_1 - 3\right) + \frac{\mu_2}{2}\left(I_3^{-2/3}I_2 - 3\right) + \frac{\kappa}{2}\left(I_3^{1/2} - 1\right)^2 + W_m^{fb}(I_m), \tag{7.1}$$

where μ_1, μ_2, and κ are the constant parameters corresponding to the Mooney-Rivlin model, and

$$W_m^{fb} = \begin{cases} \alpha_m(I_m^{1/2} - 1)^{\beta_m} & \text{if } \lambda_m > 1, \\ 0 & \text{if } \lambda_m \le 1, \end{cases}$$

with $\alpha_m, \beta_m > 0$ also constants.

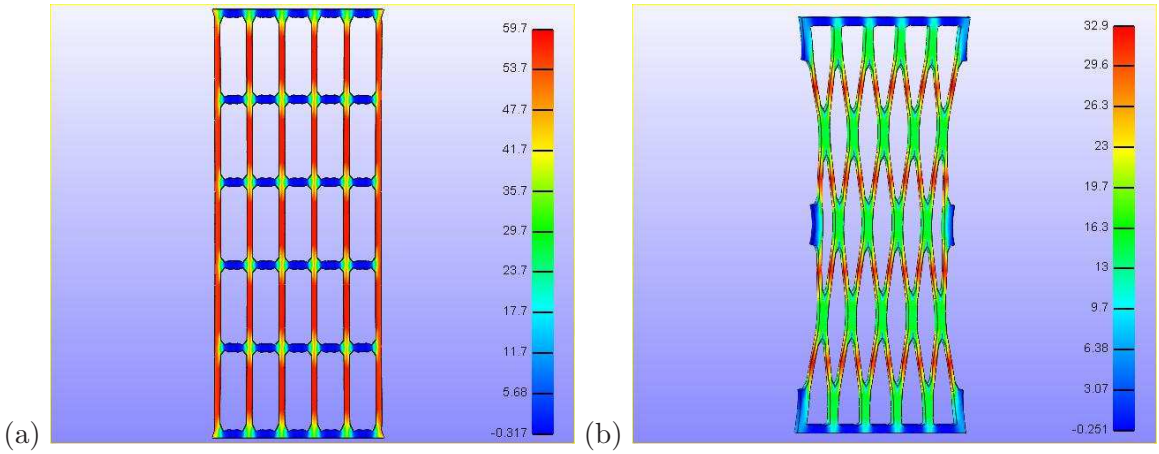

Figure 27: Vertical extension and stresses in cellular structure with (a) stacked and (b) staggered cells reinforced with vertical fibres. For the stacked cells, the deformation is almost uniform, while the staggered cells become hexagonal.

For the two-dimensional structures, we first evaluate the effect of fibre reinforcement along the vertical direction when a structure is subjected to vertical extension. Employing the SDP, by analogy to the case discussed in Section 3, we find that, due to the presence of vertical fibres, additional vertical stresses are introduced, compared to which the horizontal stresses are almost zero. Thus $\mathbf{F} = \mathbf{F}'$, and an almost uniform deformation of the cellular body with higher vertical stresses than in the non-reinforced case is expected, as illustrated in Figure 27.

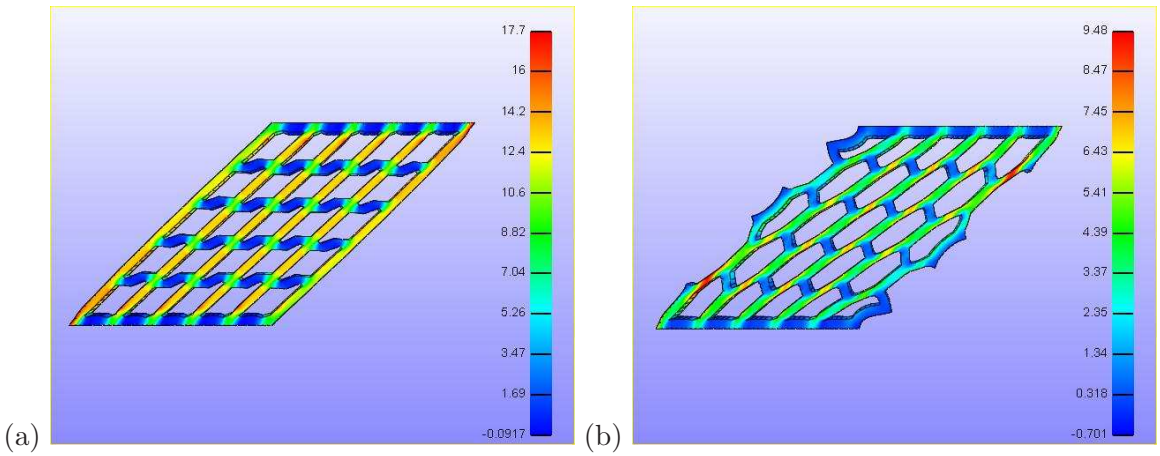

Figure 28: First principal stresses in sheared cellular structure with (a) stacked and (b) staggered cells reinforced with (initially) vertical fibres. For the stacked cells, the deformation is almost uniform, while the staggered cells become hexagonal.

For the structures reinforced with vertical fibres, when the horizontal external faces are subject to the simple shear (2.9), by a similar argument, the deformation of the cellular body is almost uniform, as shown in Figure 28.

8 Conclusion

Many fabricated or natural cellular materials are flexible, pliable structures, which resist plastic damage and fracture, and the material recovers completely after large deformations. In our study, we treat the nonlinear deformation of the elastic cell walls within the finite strain range, and identify some situations which are not displayed in the small strain regime. As expected, greater flexibility in the cell wall material leads to more flexible structures, a feature which can be observed in many softer, living or manufactured, cellular bodies. Moreover, for these materials to be serviceable, they must have the ability to carry loads that may come from arbitrary directions.

Notably, we find that, *under uniform external loading conditions, internal finite elastic deformations are typically non-uniform*, with some cells deforming more than others, and therefore the behaviour of a large structure cannot be inferred from the local behaviour at the cell level. Nonetheless, in some cases, the qualitative mechanical behaviour of the structure can be predicted from the cells geometry and the elastic properties of the underlying material by employing suitable strategies. The *successive decomposition procedure* (SDP) for large deformations of cellular structures proposed here enabled us to identify local non-uniform mechanical effects which appear in thin square or tubular cellular bodies when subject to fundamental deformations that form the basis of all other deformations, namely extension, compression, shear, and torsion, and to explore the physical properties that influence them.

In particular, *there is non-uniform deformation in uniaxial tension*, which is not observed when the elasticity of the cell walls is linear. This effect may become important when there is also a dissipative flow of liquid present between the cell walls. In uniaxial compression, axisymmetric (barrelling) as well as asymmetric (buckling) finite deformations are possible. While nature tends to load materials in tension, man-made materials are more often loaded in compression, and their elastic resistance to buckling is a very important property in manufactured soft, cushioning materials.

By the polar decomposition theorem, a simple shear (which is also the local deformation in simple torsion) is equivalent to an extension compression in the principal directions. However, in finite deformation, these directions will change with the magnitude of the deformation, whereas in linear elasticity they remain fixed. Consequently, when simple shear loading conditions are imposed on a cellular structure with hyperelastic walls, the relaxation of these conditions at the cell walls generates a non-uniform expansion in the direction orthogonal to the direction of the imposed load. This is

important for the behaviour of cellular materials submitted to more general loading conditions, *e.g.* bending of protective materials.

As a supplement to the theoretical mechanical analysis, we simulate computationally the finite elastic deformation of representative model structures with a small number of cells, such that the size of each cell and the size of the structure are comparable, and therefore the mechanical effects at the cell level are also visible at the structural level. While these computer simulations require a particular constitutive model for the cell wall material to be chosen as well, the proposed successive decomposition procedure, which is not restricted by the specific elastic material or number of cells, indicates that analogous finite deformation effects may be obtained also in other physical or computer models.

Acknowledgements

AG is a Wolfson/Royal Society Merit Award Holder and acknowledges support by the Marie Curie European Reintegration Grant BKRVRG0. The support for LAM by the Institute of Mathematics and its Applications (IMA) grant SGS10/13 is also gratefully acknowledged.

References

[1] SS Antman, Nonlinear Problems in Elasticity, Springer, 2005, Second Edition.

[2] M Baker, JL Ericksen, Inequalities restricting the form of stress-deformation relations for isotropic elastic solids and Reiner-Rivlin fluids, Journal of the Washington Academy of Sciences (1954) 44, 24-27.

[3] D Bigoni, Nonlinear Solid Mechanics. Bifurcation Theory and Material Instability, Cambridge University Press, 2012.

[4] P-O Chen, J McKittrick, MA Meyers, Biological materials: Functional adaptations and bioinspired designs, Progress in Materials Science (2012) 57, 1492-1704.

[5] M Destrade, JG Murphy, G Saccomandi, Simple shear is not so simple, International Journal of Non-Linear Mechanics (2012) 47, 210-214.

[6] JL Ericksen, Deformation possible in every compressible isotropic perfectly elastic materials, Journal of Mathematics and Phyics (1955) 34, 126-128.

[7] RA Fosdick, RT Shield, Small bending of a circular bar superposed on finite extension or compression, Arch. Ration. Mech. Anal. (1963) 12, 223-248.

[8] LJ Gibson, Biomechanics of cellular solids, Journal of Biomechanics (2005) 38, 377-399.

[9] LJ Gibson, MF Ashby, Cellular Solids: Structure and Properties, Cambridge University Press, 1997, Second Edition.

[10] LJ Gibson, MF Ashby, BA Harley, Cellular Materials in Nature and Medicine, Cambridge University Press, 2010.

[11] A Goriely, R Vandiver, M Destrade, Nonlinear Euler buckling, Proceedings of the Royal Society A (2008) 464, 3003-3019.

[12] AE Green, JE Adkins, Large Elastic Deformations (and Non-linear Continuum Mechanics), Oxford University Press, 1970, Second Edition.

[13] AE Green, RT Shield, Finite extension and torsion of cylinders, Proceedings of the Royal Society A (1951) 244, 47-86.

[14] PA Janmey, ME McCormick, S Rammensee, JL Leight, PC Georges, FC MacKintosh, Negative normal stress in semiflexible biopolymer gels, Nature Materials (2006) 6, 48-51.

[15] P. Le Tallec, Numerical methods for three-dimensional elasticity. In Handbook of Numerical Analysis (eds PG Ciarlet, JL Lions), vol. 3., Elsevier Sciences B.V., Amsterdam, 1994, 465-622.

[16] VA Lubarda, Constitutive theories based on the multiplicative decomposition of deformation gradient: Thermoelasticity, elastoplasticity, and biomechanics, Applied Mechanics Review (2004) 57, 95-108.

[17] SA Maas, BJ Ellis, GA Ateshian, JA Weiss, FEBio: Finite Elements for Biomechanics, Journal of Biomechanical Engineering (2012) 134.

[18] S Marzano, An interpretation of Baker-Ericksen inequalities in uniaxial deformation and stress, Meccanica (1983) 18, 233-235.

[19] MA Meyers, P-Y Chen, AY-M Lin, Y Seki, Biological materials: Structure and mechanical properties, Progress in Material Science (2008) 53, 1-206.

[20] P Michailides, N Triantafyllidis, JA Shaw, DS Grummon, Superelasticity and stability of a shape memory alloy hexagonal honeycomb under in-plane compression, International Journal Solids & Structures (2009) 46, 2724-2738.

[21] LA Mihai, A Goriely, Positive or negative Poynting effect? The role of adscititious inequalities in hyperelastic materials, Proceedings of the Royal Society A (2011) 467, 3633-3646.

[22] LA Mihai, A Goriely, Numerical simulation of shear and the Poynting effects by the finite element method: An application of the generalised empirical inequalities in non-linear elasticity, International Journal of Non-Linear Mechanics (2013) 49, 1-14.

[23] LA Mihai, A Goriely, Nonlinear Poisson effects in soft honeycombs, Proceedings of the Royal Society A (2014) 470, article number 20140363.

[24] RW Ogden, Non-Linear Elastic Deformations, Dover, 1997, Second Edition.

[25] PM Rich, Mechanical architecture of arborescent rain forest palms, Principes (1986) 30, 117-131.

[26] MG Scanlon, Biogenic cellular solids. In JR Dutcher, and AG Marangoni (eds.), Soft Materials: Structure and Dynamics, New York: Marcel Dekker, 2005, 321-349.

[27] S Shan, SH Kang, P Wang, C Qu, S Shian, ER Chen, K Bertoldi, Harnessing multiple folding mechanisms in soft periodic structures for tunable control of elastic waves, Advanced Functional Materials (2014) 24, 4935-4942.

[28] RT Shield, Deformations possible in every compressible, isotropic, perfectly elastic material, Journal of Elasticity (1971) 1, 91-92.

[29] MH Siboni, PP Castaeda, Fiber-constrained, dielectric-elastomer composites: Finite-strain response and stability analysis, Journal of the Mechanics and Physics of Solids (2014) 68, 211-238.

[30] C Truesdell, W Noll, The Non-Linear Field Theories of Mechanics, Springer-Verlag, 2004, Third Edition.

[31] P Wang, F Casadei, S Shan, JC Weaver, K Bertoldi, Harnessing buckling to design tunable locally resonant acoustic metamaterials, Physical Review Letters (2014) 113, article number 014301.

[32] D Wang, MS Wu, Generalized shear of a soft rectangular block, Journal of the Mechanics and Physics of Solids (2014) 70, 297-313.

[33] D Weaire, MA Fortes, Stress and strain in liquid and solid foams, Advances in Physics (1994) 43, 685-738.